UNIVERSITY OF Nebraska Lincoln

THE UNIVERSITY OF IOWA

KU THE UNIVERSITY OF KANSAS

MISSOURI S&T

LINCOLN UNIVERSITY MISSOURI

NICC NEBRASKA INDIAN COMMUNITY COLLEGE

UNIVERSITY OF Nebraska Omaha

University of Nebraska Medical Center

KU MEDICAL CENTER The University of Kansas

Development of New Design Guidelines for Protection against Erosion at Bridge Abutments - Phase IV

George Constantinescu, PhD

Professor
Department of Civil and Environmental Engineering
The University of Iowa

Hao Wu

Graduate Research Assistant
Department of Civil and Environmental Engineering
The University of Iowa

THE UNIVERSITY OF IOWA

2021

MATC

Development of New Design Guidelines for Protection against Erosion at Bridge Abutments - Phase IV

George Constantinescu, Ph.D., PI
Professor
Department of Civil and Environmental Engineering
The University of Iowa

Hao Wu
Graduate Research Assistant
Department of Civil and Environmental Engineering
The University of Iowa

Technical Report Documentation Page

1. Report No. 25-1121-0005-141-4	2. Government Accession No.	3. Recipient's Catalog No.
4. Title and Subtitle Development of New Design Guidelines for Protection against Erosion at Bridge Abutments - Phase IV		5. Report Date December 2021
		6. Performing Organization Code
7. Author(s) George Constantinescu, Ph.D., PI ORCID: 0000-0001-7060-8378 Hao Wu		8. Performing Organization Report No. 25-1121-0005-141-4
9. Performing Organization Name and Address Department of Civil and Environmental Engineering The University of Iowa Iowa City, IA 52242		10. Work Unit No.
		11. Contract or Grant No. 69A3551747107
12. Sponsoring Agency Name and Address Mid-America Transportation Center 2200 Vine St. PO Box 830851 Lincoln, NE 68583-0851		13. Type of Report and Period Covered Final Report Jan 2021 - Dec 2021
		14. Sponsoring Agency Code MATC TRB RiP No. 91994-79
15. Supplementary Notes Conducted in cooperation with the U.S. Department of Transportation, Federal Highway Administration.		

16. Abstract

Maintaining road operations requires reliable and safe transportation infrastructure design, in particular for bridges that need to remain operational during floods and other extreme weather events. A numerically based investigation is carried out to determine the minimum median diameter of the riprap stone needed to avoid shear failure inside the riprap apron used to protect spill-through abutments against erosion. The Year 4 report uses results of simulations conducted with variable floodplain width, riprap size, channel curvature and length of the spill-through abutment to propose a new two-parameter design formula for riprap size selection for spill-through abutments placed in straight or curved compound channels. The report also discusses how the flow structure and bed shear stress distributions vary with increasing flow depth in between free-surface (FS) flow and pressurized flow (submerged orifice or overtopping) conditions in a straight channel containing wing-wall abutments protected by a riprap apron. This data is critical to propose corrections to existing design formulas for riprap size selection which were developed for the open-channel flow regime such that estimates of the critical Froude number can be provided for cases when the bridge deck becomes submerged at high flow conditions.

17. Key Words Bridges, Bridge scour, Bridge abutment, Local Scour, Rip-rap protection against scour		18. Distribution Statement No restrictions. This document is available through the National Technical Information Service, Springfield, VA 22161.	
19. Security Classif. (of this report) Unclassified	20. Security Classif. (of this page) Unclassified	21. No. of Pages 49	22. Price

Form DOT F 1700.7 (8-72) Reproduction of completed page authorized

Table of Contents

List of Figures

List of Tables

Acknowledgments

Disclaimer

The contents of this report reflect the views of the authors, who are responsible for the facts and the accuracy of the information presented herein. This document is disseminated in the interest of information exchange. The report is funded, partially or entirely, by a grant from the U.S. Department of Transportation's University Transportation Centers Program. However, the U.S. Government assumes no liability for the contents or use thereof.

Abstract

Severe floods in the United States Midwest have caused major erosion at bridge abutments despite their protection design measures following existing guidelines (e.g., HEC 23, 2001 and following updates through 2009). At high-flow conditions, erosion occurs not only inside the main channel but also over its floodplains, especially in the region of flow contraction induced by the presence of obstructions such as bridge piers, bridge abutments, and the attached embankments (Sturm and Janjua, 1994; Sumer and Fredsoe, 2002). Severe scour can endanger the stability of the embankment and induce scour beneath the foundations of the abutments. Placing riprap stone around the base of each abutment and over its erodible faces is the most common way to protect abutments against erosion (e.g., see NCHRP Projects 24-18, 24-19, 24-20). One likely possibility for the severe local scour observed at many abutments is that existing design formulas to calculate the minimum size of the riprap stone used for protection of wing-wall and spill-through abutments (Lagasse et al., 2001; Pagan-Ortiz, 1991) are based on an oversimplified approach. Moreover, such formulas do not account for complexities associated with these structures being placed in natural streams where, for instance, bank curvature effects may be important. The coefficients in these formulas were determined based on a limited series of laboratory experiments conducted for a relatively narrow range of relevant geometrical and flow parameters that influence the capacity of the flow to induce erosion at such bridge sites. Another limitation of present design formulas is that they can be applied only for open channel flow (free surface, FS) regime at the bridge site. However, the most severe scour around the abutments occurs when the bridge deck becomes submerged and the flow regime becomes pressurized (e.g., submerge orifice, SO or overtopping, OT).

This project aims to improve the performance and range of applicability of riprap design formulas used for erosion protection at wing-wall and spill-through abutments. The mean flow fields and the bed shear stress distributions are obtained from fully three-dimensional, non-hydrostatic RANS simulations. These data are then used to estimate the maximum bed shear stress over the riprap apron, the shear-failure entrainment threshold for the riprap stone and the other variables in the design formulas recommended in HEC 23. The approach was validated for the case of wing-wall abutments placed in a straight channel based on data from laboratory experiments. The present Year 4 report uses results of simulations conducted with variable floodplain width, riprap size, channel curvature and length of the spill-through abutment to propose a new two-parameter design formula for riprap size selection for spill-through abutments placed in straight or curved compound channels. The report also discusses how the flow structure and bed shear stress distributions vary with increasing flow depth in between free-surface (FS) flow and pressurized flow (submerged orifice, SO or overtopping, OT) conditions in a straight channel containing wing-wall abutments protected by a riprap apron. This data is critical to propose corrections to existing design formulas for riprap size selection developed for the free surface regime such that estimates of the critical Froude number for riprap shear failure can be provided for cases when the bridge deck becomes submerged at high flow conditions.

Chapter 1 Introduction

1.1 Motivation and Proposed Approach

Reliable and safe transportation infrastructure design for flooding events is a main task for state and federal agencies in charge of maintaining our roads to remain operational. The US Midwest has experienced increasingly catastrophic flood events over the last few decades. Severe erosion problems were reported at many bridge sites, especially for abutments and embankments of smaller-size bridges. Severe scour can endanger the stability of the embankment and induce scour beneath the foundations of the abutments. In extreme cases, this may lead to bridge failure which results in interrupting the traffic and, in some cases, loss of human life. Two of the most encountered types of abutments used at bridges are spill-through and wing-wall abutments.

Considerable progress has been made over the two decades in understanding the mechanisms of local scour at abutments and in developing effective bridge-scour countermeasures to protect these structures against severe erosion (Sumer and Fredsoe 2002; Melville and Coleman 2000; Dey and Barbhuiya 2005; Kothyari at al. 2007; Sturm et al. 2011; Ettema et al. 2011, 2015, 2017; Koken and Constantinescu 2014; Hong and Abid 2019). Placing riprap stone around the base of a bridge abutment, where the highest stresses generally occur, and over its erodible faces is one of the most common ways to protect abutments against erosion (Brown and Clyde 1989; Melville and Coleman 2000). The riprap stone provides an armor layer protection to the finer sediments present near the bed surface. When placed near the base of an abutment, the main effect of the apron is to modify the geometry of the scour hole such that the maximum scour depth is reduced and the locations of large scour move away from the base/toe of the abutment.

The riprap stone forming the abutment apron may be subjected to several modes of failure including shear failure, winnowing failure, and edge failure (Melville et al. 2007). In general, the minimum size of the riprap stone in design equations is determined such that shear and edge failure are avoided (Chiew 1995; Melville et al. 2007; Barkdoll et al. 2007). Shear failure occurs where the individual riprap stones are not large enough to resist entrainment by the flow. In general, design guidelines for bridge piers and abutments (Hoffmans and Verheij, 1997; Lagasse et al. 2001; Sumer and Fredsoe 2002; Melville and Coleman 2000; Melville et al., 2006a, 2006b; Cardoso et al. 2010) are mostly based on laboratory experiments (flume studies) conducted for a limited range of flow conditions (e.g., straight channels, limited width of the floodplain). None of these design formulas can be used for cases when bank curvature effects are important or pressure scour effects due to bridge deck submergence are present. Another general characteristic of most existing design formulas for bridge abutments is the minimum size of the median diameter of the riprap stone, D_{50}, in these formulas is only a function of the Froude number defined with the mean velocity in the contracted region containing the abutment and the flow depth. The effects of important geometrical parameters that affect the flow and its capacity to entrain sediment near bridge abutments (e.g., the floodplain width and the relative abutment length in the case of spill-through abutments) are not accounted for in these formulas. Thus, there is a need to improve these guidelines and propose modified formulas or methodologies that can provide effective protection against erosion for a larger range of flow and geometrical conditions at these two types of abutments. There is also a need to understand how the critical Froude number changes once the flow beneath the bridge deck becomes pressurized, which should lead to proposing corrections on how existing design formulas can be used for pressurized

flow regime. Such information is critical, as most of the local scour occurs at high flow conditions when the bridge deck becomes submerged.

One possible alternative to flume studies is to use numerical simulations to estimate the boundary shear stress over the channel bed, including over the regions protected by rock riprap. Fully 3-D, non-hydrostatic Reynolds-Averaged Navier-Stokes (RANS) models using two-equation turbulence closures are generally quite successful to predict flow and bed shear stress distributions in natural channels containing hydraulic structures (Roulund et al. 2005). Such models can account for the effect of the bed roughness on the flow and turbulence inside the channel (Zeng et al. 2008). For cases when the flow becomes pressurized at the bridge, the free surface position is part of the solution and the rigid lid approach cannot be used. For such cases, the Volume of Fluid (VOF) method can be used to predict the free surface together with the flow field and bed shear stresses over the riprap apron.

If such a numerical approach is adopted, a series of 3-D simulations may be used to determine whether the riprap stone inside the apron will fail or not. For a given channel and abutment geometry, incoming flow discharge and flow depth, the predicted maximum shear stress over the riprap region is compared with the critical value for riprap failure to determine if the riprap stone will be entrained into the water column or not. To estimate the critical Froude number corresponding to the shear-failure entrainment threshold for the riprap stone, the discharge is then varied until the maximum bed shear stress over the riprap region is equal to the critical value. The procedure is the same for cases with free surface and pressurized flow regimes at the bridge site containing the abutments.

1.2 Prior Main Results and Findings

Figure 1.1 shows the general layout of the computational domain and the main geometrical variables (B_f=floodplain width, L_a=abutment length, y_m=flow depth over main channel, y_f=flow depth over the floodplains), as well as the position of the riprap apron. Outside of the riprap apron, the flat bed was covered with sand with d_{50}=0.82 mm. The inlet discharge was varied until the maximum value of the bed friction velocity over the riprap layer was $0.35u_{*cr}$, where u_{*cr} is obtained from the Shields diagram for a given mean diameter of the riprap stone, D_{50}. Following Melville and Coleman (2000), this value was used to determine the riprap shear failure entrainment threshold. The Froude number, Fr, was calculated using the mean velocity in the section containing the abutment.

The main research activity conducted during Year 1 was the validation of the method using the experimental data of Melville et al. (2007) for wing-wall abutments placed in a straight channel (fig. 1.1a). Simulations were conducted with flow only inside the main channel (y_m=0.1 m) and with flow over the floodplain (y_m=0.17 m, y_f=0.07 m) for B_f=0.4 m, 1.4 m, and 20 m and for 20 mm<D_{50}<61 mm. Five of the simulated test cases of the wing-wall abutment corresponded to those in the experiments of Melville et al. (2007). Figure 1.2 shows that for each of the five series of experiments, the numerically predicted shear failure entrainment threshold was situated in between the limiting experiments where no shear failure and shear failure, respectively, were observed.

During Year 2, a comprehensive parametric study was conducted for straight and curved channels containing wing-wall abutments at their two banks. The general layout is shown in figure 1.3. Simulations were conducted for normal flow conditions (y_m=0.1 m) and with flow over the floodplains (y_m=0.17 m, y_f=0.07 m) and with varying riprap diameter (D_{50}=20 mm, 28

mm, 40 mm and 60 mm), floodplain width (B_f/W=0, 0.2 and 0.7), and channel radius of curvature (R/W=∞, 20, 10 and 1), where W=2 m is the width of the main channel. Using these data, the performance of existing design formulas (Pagan-Ortiz 1991; Lagasse et al. 2001) for riprap protection at bridges containing wing-wall abutments was checked for a wide range of conditions, outside of the range used to calibrate these formulas. A main finding was the two design formulas are not conservative enough for straight channels with a large floodplain width (Case III in fig. 1.4a). The design formulas were also found not to be conservative enough for cases where the abutments were placed in channels with a relatively high curvature (R/W<20).

a)   b)

Figure 1.1 Sketch showing general layout of the preliminary numerical simulations performed for a wing-wall abutment (left) and for a spill-through abutment (right) placed on the floodplain of a straight channel. Dimensions are in meters. The wing-wall abutment geometrical set up corresponds to that used in the laboratory experiments of Melville et al. (2007). Reproduced from Wu et al. (2020a) and Wu et al., (2020b).

Figure 1.2 Validation of the numerical predictions of riprap shear failure for a wing-wall abutment placed in a straight channel. Also shown are predictions using the Lagasse et al. (2001) and Pagan-Ortiz (1991) equations and the experimental data of Melville et al. (2007). Simulation data (red squares) show predicted conditions for treshold of riprap entrainment by shear failure. Experimental data only show if shear failure occurred (open symbols) or not (solid symbols) in the corresponding experiments. Reproduced from Wu et al. (2020a).
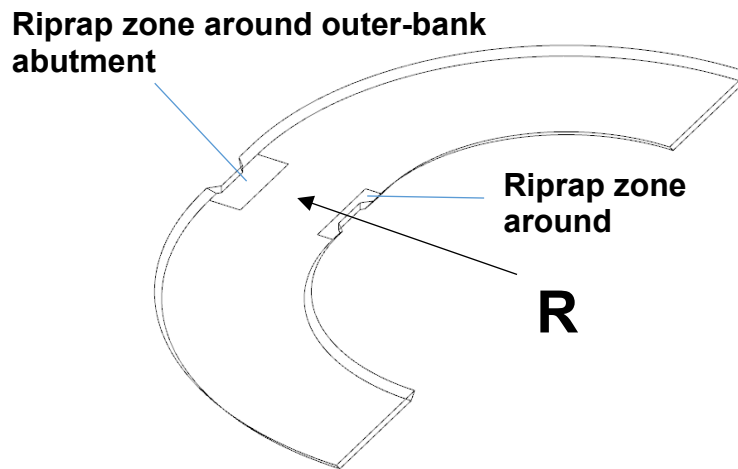
Figure 1.3 Sketch showing general layout used in the simulations performed in a curved channel containing an abutment at each bank. The channel radius of curvature is R.

6
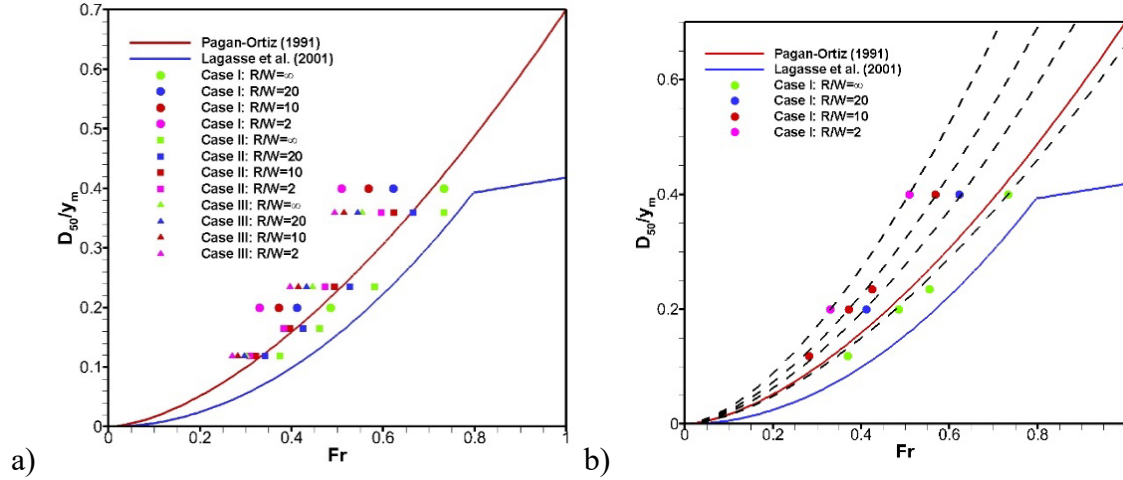
Figure 1.4 Comparison of numerical results with Lagasse et al. (2001) and Pagan-Ortiz (1991) equations for wing-wall abutments placed in straight and curved channels. The floodplain width is $B_f/W=0$ for Case I, $B_f/W=0.2$ for Case II and $B_f/W=0.7$ for Case III. Simulation data show predicted conditions for treshold of riprap entrainment by shear failure. The dashed lines in frame b show the new design formula predictions for Case I simulations. Partially reproduced from Wu et al. (2020a).

The other main contribution of Year 2 was to propose a new design formula that retains the same functional relationship as that of Pagan-Ortiz (1991) and Lagasse et al. (2001) formulas:

$$D_{50}/y=(K_s/(S_s-1))^{0.5\alpha} *Fr^\alpha=C^{0.5\alpha}*Fr^\alpha \qquad (1.1)$$

where K_s is the shape factor, $S_s=2.65$ is the specific gravity of the riprap stone, $C=K_s/(S_s-1)$ is a model coefficient and Fr is defined with the mean velocity in the section containing the abutments, V, and a characteristic length scale, y. For wing-wall abutments, $y=y_m$. Using this formulation, $C=0.645$ and $\alpha =1.62$ for the Pagan-Ortiz (1991) formula and $C=0.618$ and $\alpha =2.0$ for the Lagasse et al. (2001) formula (Fr<0.8). In the new design formula for wing-wall abutments, C and α are a function of the main nondimensional geometrical parameters (e.g.,

7

B_f/W, R/W). The recommended values of C and α are summarized in table 1.1. More details are given in Wu et al. (2020a). One major finding was that α is not a function of the channel curvature, R/W, but increases monotonically with increasing B_f/W. The predicted range for α (1.62<α<1.84) was in between the values used by the Pagan-Ortiz (1991) formula (α=1.62) and Lagasse et al. (2001) formula (α=2).

Table 1.1 Best fit values of the power coefficient α and of the coefficient C as a function of the nondimensional radius of curvature R/H_{ref} and floodplain width, B_f/H_{ref} for a wing-wall abutment.

	$R/H_{ref}=\infty$	$R/H_{ref}=400$	$R/H_{ref}=200$	$R/H_{ref}=40$
	$R/W=\infty$	$R/W=20$	$R/W=10$	$R/W=2$
$B_f/H_{ref}=0.0$	α=1.62	α=1.62	α=1.62	α=1.62
$B_f/W=0$	C=0.60	C=0.82	C=0.99	C=1.25
$B_f/H_{ref}=4.0$	α=1.67	α=1.67	α=1.67	α=1.67
$B_f/W=0.2$	C=0.54	C=0.65	C=0.75	C=0.81
$B_f/H_{ref}=14.0$	α=1.84	α=1.84	α=1.84	α=1.84
$B_f/W=0.7$	C=1.07	C=1.11	C=1.24	C=1.32

The main contribution of Year 3 was to propose a new design formula for spill-through abutments positioned on the floodplain of straight channels. This new formula also assumes the form of eqn. (1.1) and its two coefficients are a function of the nondimensional abutment length L_a/B_f, and the floodplain width, B_f/H_{ref}. For spill-through abutments, Lagasse et al. (2001) formula for Fr<0.8 corresponds to C=0.54 and α=2 in eqn. (1.1) while Pagan-Ortiz (1991) formula corresponds to C=0.324 and α=2.
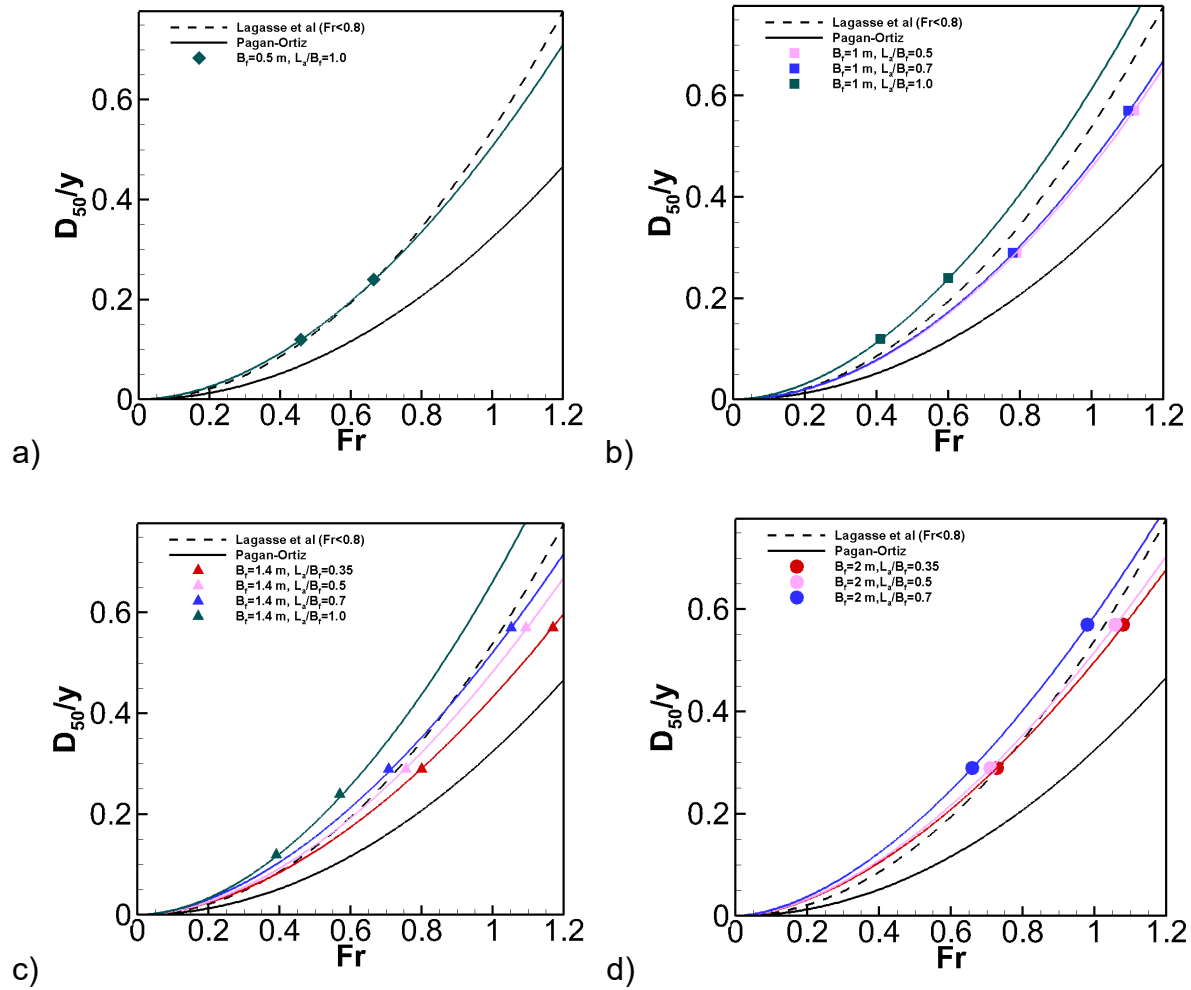
Figure 1.5 Comparison between the numerical predictions of the critical Froude number and Lagasse et al. (2001) and Pagán-Ortiz (1991) equations for spill-through abutments in straight. a) B_f/H_{ref}=5; b) B_f/H_{ref}=10; c) B_f/H_{ref} =14; d) B_f/H_{ref} =20. The colored lines show eqn. (1.1) predictions of the critical Froude number using best fit values of C and α.

Results in figure 1.5 show that the Pagan-Ortiz formula is not conservative enough for all cases. The Lagasse et al. (2001) formula does much better; however, it still overpredicts the critical Froude number for cases with relatively large L_a/B_f. Its performance is much better for low B_f values (e.g., the formula is conservative enough for B_f=0.5 m). Results in figure 1.5 also show that for constant D_{50}/y, Fr increases monotonically with decreasign L_a/B_f, an effect not

9

captured by existing design formulas. Another interesting result is that α=1.85 for all cases with

L_a/B_f=1 (abutment ressembles a wing-wall abutment) with C increasing with increasing B_f. For

0.3<L_a/B_f<0.8, α is independent of L_a/B_f and C increases with increasing L_a/B_f. The predicted

range of α was 1.7-1.95, slightly lower than the value, α=2, in the Lagasse et al. and Pagan-Ortiz

formulas.

1.3 Objectives

The main research objectives for Year 4 were to:

1.   Extend the two-parameter design formula developed during Year 3 for cases when the

spill-through abutments are positioned on the floodplains of a curved channel;

2.   Develop and test a Volume of Fluid based model that can be used to predict flow and free

surface position in compound channels containing the bridge abutments and the bridge structure

(e.g., the bridge deck). Such a model is needed for cases when the flow is pressurized at the

bridge site;

3.   Investigate how the flow, bed shear stress distributions, and the critical Froude number

vary with increased flow depth in the incoming flow as the flow regime changes from free

surface to pressurized beneath the deck of a bridge containing two wing-wall abutments placed

in a straight compound channel. The investigation should be conducted with different flow

depths in the approach flow and diameters of the riprap stone and should include cases when the

bridge deck supported by the abutment is fully (overtopping regime) or partially submerged

(orifice flow regime).

1.4 Justification of Research Approach

        Understanding and being able to quantitatively describe how the hydrodynamics of the stream flow field (velocity magnitude and bed shear stress distributions around the bridge site) changes with increasing stage and discharge as a result of a flood is critical to be able to propose effective measures to protect bridge abutments and piers against erosion. The National cooperative Highway Research Program Report 587 (NCHRP Report 587) used in the development of HEC 23 (2001, 2009) states the following:

> Selection of countermeasures to protect bridges from scour requires estimates of velocity distributions in the bridge opening. Estimates of the peak velocity in what is typically a highly non-uniform flow distribution near the tip of the abutment is necessary to determine whether countermeasures are necessary and, if so, to determine the type, size, and extent of countermeasures to protect bridge abutments from scour. Laboratory physical models have been developed to determine the size, type, and location of protection for a relatively small range of flow conditions at bridges; however, the laboratory models represent very simplistic geometric conditions. Effective transfer of laboratory model results to the complex hydrodynamic conditions of real bridge sites requires that flow velocity be predicted in the vicinity of bridge abutments using numerical models.

        The report also comments on the limitations of the two-dimensional (2-D) depth-averaged modeling approach which was used in past studies to provide more accurate estimations of the variables in the design formulas used to protect against erosion. The main limitations of the 2-D approach are due to the hydrostatic pressure assumption and simplified turbulence modeling. Moreover, the region of maximum velocity amplification near the abutment toe is generally located in a region of high flow curvature where 2-D numerical models are not very accurate.

        The present study uses fully three-dimensional (3-D), non-hydrostatic, RANS simulations performed on fine meshes to obtain the 3-D mean velocity flow field. This allows direct estimation of the mean boundary shear stress over the whole bed region, including over the

riprap apron. For cases when the flow becomes pressurized near the bridge, Volume of Fluid (VOF) RANS simulations are performed due to the need to predict the free surface position as part of the solution.

Given the detailed information on the flow fields, turbulence and their effects on the bed shear stress distributions available from such 3-D simulations, the proposed approach can lead to extension of the range of geometrical and flow configurations for which design formulas can be applied (e.g., abutments placed inside or immediately downstream of curved channels, high flow conditions that lead to the bridge deck becoming submerged). For such cases, laboratory experiments are very expensive and the range of geometrical (e.g., channel aspect ratio, width of the floodplain) and flow parameters in these experiments are even more limited compared to the canonical case of an abutment placed in a straight channel. The numerically based approach adopted in the present study does not face these limitations. Moreover, the numerical approach can be applied for cases when the flow regime changes from free surface to pressurized at the bridge, a fairly common situation during high flow events (floods) when the most severe local scour is generally observed near the bridge abutments.

Chapter 2 Numerical Method

STAR-CCM+ is a state-of-the-art commercial code developed by CD-Adapco which solves the fully 3-D non-hydrostatic Navier-Stokes equations together with the turbulence model equations. The solver uses the finite-volume method to integrate the governing equations and allows the use of unstructured meshes. The RANS turbulence model provides the value of the eddy viscosity. The governing continuity and momentum equations are:

$$\frac{\partial U_i}{\partial x_i} = 0 \qquad (2.1)$$

$$\frac{\partial U_i}{\partial t} + \frac{\partial (U_i U_k)}{\partial x_k} = -\frac{1}{\rho}\frac{\partial P}{\partial x_i} + \frac{1}{\rho}\frac{\partial}{\partial x_k}\left[(\mu + \mu_t)\left(\frac{\partial U_i}{\partial x_k} + \frac{\partial U_k}{\partial x_i}\right)\right] - g\hat{k} \qquad (2.2)$$

where

U_i = Reynolds Averaged velocity component along the i direction

ρ = fluid density

μ = molecular dynamic viscosity

μ_t = eddy viscosity calculated from the RANS turbulence model

P = pressure

g = gravitational acceleration

$\hat{k}$ = unit normal vector along the vertical direction

The discretised Navier-Stokes equations are solved using a fractional-step algorithm. The advective terms are discretised using the second-order accurate upwind scheme, while the transient term discretization in time is second-order accurate based on an implicit representation.

The diffusive terms and the pressure gradient terms are discretised using the second-order accurate central scheme. The pressure-coupling is achieved using the SIMPLE algorithm. In the SIMPLE algorithm, the momentum equations without the pressure gradient term are advanced in time and an intermediate velocity is obtained which does not satisfy the continuity equation. A pressure-correction algorithm is then employed to modify the pressure field such that mass conservation is achieved.

Several two-equation turbulence models available in STAR-CCM+ were initially considered. The k-w SST model performed more accurately for channel flow simulations with a large value of the relative bed roughness, leading to its use in the simulations reported in this paper. STAR-CCM+ with the k-w SST turbulence model was widely used and validated for predictions of flow in channels containing hydraulic structures (Cheng et al. 2018), including for cases when an unsteady flood wave advanced in a channel with natural bathymetry (Cheng et al. 2018; Horna-Munoz and Constantinescu 2018, 2020).

For simulations with a deformable free surface, the Volume-of-Fluid (VOF) method is used to track the location of the free surface. A layer of air is present over the parts of the domain that contain, or can contain, water during the simulation. The VOF method is based on the advection of the volume fraction of water, α, for which a standard advection equation ($\frac{\partial \alpha}{\partial t} + U_j \frac{\partial \alpha}{\partial x_j} = 0$) is solved. In cells fully occupied by water $\alpha=1$, while in cells containing only air $\alpha=0$. The advection term in the VOF equation is discretised using the second-order upwind scheme. The temporal discretization is second order accurate.

No-slip boundary conditions were specified at all wall boundaries. The bed shear was calculated using the law of the wall for rough surfaces. At the rough-wall boundaries, the specified value of the surface roughness k_s was different over the riprap region ($k_s=D_{50}$) and over

the rest of the channel bed that was assumed to be covered by a layer of sand ($k_s=d_{50}$). The bed shear stress is estimated using the law of the wall for rough surfaces.

Preliminary straight and curved channel flow and steady RANS simulations with periodic boundary conditions in the streamwise direction were performed to obtain a fully developed channel flow solution to be used to specify the inlet boundary condition in the corresponding simulations of flow in compound channels containing an abutment on each floodplain. The cross section of the channel used in the preliminary simulations was identical to the inlet section of the computational domain in the simulations where abutments were present. The 2-D distributions of the velocity and the turbulence variables from the periodic simulations were specified at the inlet of the domain containing the abutments.

In the simulations performed with a rigid lid at the free surface, the outlet was specified as a pressure outlet boundary. Given the low value of the channel Froude number, the free surface was treated as a slip (symmetry) boundary on which the vertical velocity was set equal to zero. All simulations were performed in domains containing abutments at both sides of the channel. This is needed because in the case of curved channels the flow field is not symmetrical with respect to the axis of the main channel. The compound channel cross section was symmetrical with respect to the centerline of the main channel and the spill-through abutments placed over the two floodplains were identical.

In the VOF simulations, the height of the computational domain was larger than the flow depth inside the channel to allow for a layer of air to be present. The outlet and top (opened to air) boundaries were specified as pressure outlets. The desired pressure and volume fraction of water were directly specified on all outlet and top boundary surfaces. Specifying the distribution of the volume fraction of water is equivalent to imposing a free surface elevation at the outlet

15

boundary. In the case when air was present next to the outlet boundary or the top boundary, the pressure outlet was set to zero Pascals, and the volume fraction of water was set to $\alpha=0$. The inlet was specified as a velocity inlet with a specified level of the free surface. As VOF simulations were performed only for wing-wall abutments placed in a straight channel, the computational domain contained only one abutment and half of the channel. A symmetry boundary condition was used in the symmetry plane of the channel (lateral boundary of computational domain).

STAR-CCM+ contains a very powerful meshing capability in which an initial geometry can be imported and smoothed in such a way to improve computational efficiency without loss of critical information. Once the geometry has been processed, a volume mesh is created with the desired meshing model to obtain a high-quality mesh. The grid generator allows the use of various controls and the generation of fine meshes in different parts of the domain where flow resolution needs to be higher (e.g., near the solid surfaces to resolve the attached boundary layers), which is essential to generate a high quality mesh. One of the main advantages of the grid generator in STAR-CCM+ is that it allows automatic grid refinement in critical regions situated around the abutments with a smooth transition to regions where the mesh is coarser.

Chapter 3 Spill-Through Abutments Placed in Straight and Curved Channels

Spill-through abutments are usually set back on floodplains (fig. 1.1b). At high-flow conditions, the flow over the floodplain contracts as it enters the bridge crossing region, which generally leads to erosion developing around the toe of the abutments. For such flow conditions, the maximum scour depth at spill-through abutments that are set back from the channel's banks can attain several times the incoming flow depth over the floodplain. To reduce erosion developing at the toe of such abutments, a riprap collar is placed around each abutment's toe.

Many bridges are built inside, or immediately downstream, of regions where bank curvature is important (e.g., the ratio between the radius of curvature and the channel width is larger than 20). For such cases, the approaching velocity field around the abutment is quite different compared to the case of a straight channel, with the streamwise velocity being larger close to the abutment situated at the outer bank of the curved channel, at least for small to moderate channel curvatures. High-flow conditions, where the floodplain becomes submerged, add to the flow complexity for cases when abutments are situated inside or close to regions where the channel is not straight.

The geometry of the spill-through abutments (fig. 1.1b) is very similar to that used in the laboratory experiments of Melville et al. (2006b), while the compound channel geometry is identical to that used in the corresponding simulations conducted with wing-wall abutments. The abutment has a trapezoidal cross section. The slope of the sidewalls is 1V:2H and the bottom width of the abutment is 0.9 m. The width of the riprap apron protecting each abutment is W=0.3 m. The width of the main channel is B_m=2 m. The width of the transition region between main channel and its floodplain is 0.1 m. The difference between the bed elevation over the floodplain and over the main channel is 0.1 m. In the simulations conducted with L_a=B_f, the

riprap apron is partially situated inside the main channel. Figure 3.1 shows the computational

domain for a case when the two spill-through abutments are placed on a straight channel.

For simplicity, in the test cases performed with spill-through abutments the channel

radius of curvature is assumed to be constant and the nondimensional ratio of curvature is

defined as the ratio between the radius of curvature of the main channel centerline, R, and the

width of the main channel, B_m.

For each simulation, the inlet section was situated at a distance L_{x1} that was larger than

$4B_f$ from the abutments. The distance between the abutments and the exit section, L_{x2}, was

sufficiently large for the separated flow behind the abutments to reattach.
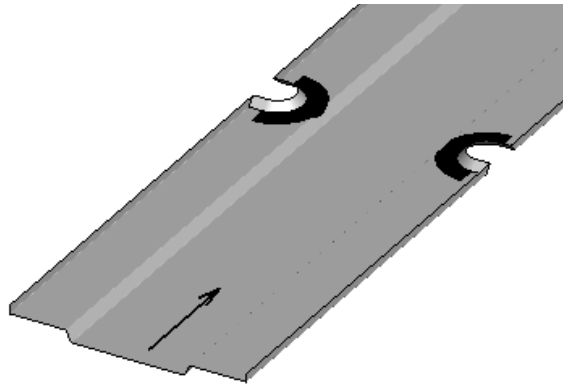
Figure 3.1 Sketch showing computational domain in the straight channel cases containing a
spill-through abutment at each bank. Also shown in black is the riprap apron around the toe of
each abutment (from Wu et al., 2020b)

3.1 Description of Test Cases and RANS Solutions

The length scale used to nondimensionalize the different variables is $H_{ref} = 0.1$ m. The

velocity scale ($V_{ref} = 0.4$ m/s) is within the range of approach flow velocities in the main channel

(0.2 m/s to 0.65 m/s). The mean diameter of the sand covering the channel bed outside of the

regions protected by riprap stone is $d_{50} = 0.82$ mm. Simulations in channels containing spill-through abutments at their sides were performed for a flow depth (y_m=0.17 m, y_f=0.07 m) corresponding to flood conditions. Simulations were conducted for four values of the floodplain width B_f/H_{ref} = 5, 10, 14, and 20. These series of simulations conducted with a constant value of B_f/H_{ref} are denoted Case I, Case II, Case III, and Case IV in table 3.1, respectively. For each case, simulations are conducted with two different values of the median diameter of the riprap stone, D_{50}/H_{ref} = 0.2 and 0.4, three values of the radius of curvature measured along the centreline of the main channel, R/H_{ref} = ∞ (straight channel) and R/H_{ref} = 400 and 200 (R/B_m = 20 and 10). The relative abutment length, L_a/B_f, varies between 0.35 and 1.0 (table 3.1).

The nondimensional values of the critical bed friction velocity for riprap shear failure were $u_{\tau c}/V$=0.12 and 0.175 for D_{50}/H_{ref}=0.2 and 0.4, respectively. The mean streamwise velocity in the cross section containing the two abutments was used to calculate the Froude number, Fr. For each test case, the inlet discharge was varied in a series of simulations until two of the simulations predicted a maximum bed shear stress over the riprap apron slightly larger and, respectively, slightly smaller than the critical value for riprap shear failure determined following the procedure outlined in Melville et al. (2007).

Table 3.1 Matrix of test cases considered for compound channels containing a spill-through abutment over each floodplain.

Test Case	B_f/H_{ref}	B_f/B_m	L_a/H_{ref}	L_a/B_f	R/H_{ref}	R/B_m	D_{50}/H_{ref}
			5	1.0	∞	∞	0.2, 0.4
Case I	5	0.25			400	20	0.2, 0.4
					200	10	0.2, 0.4
			5	0.5	∞	∞	0.2, 0.4
					400	20	0.2, 0.4
					200	10	0.2, 0.4

Test Case	B_f/H_{ref}	B_f/B_m	L_a/H_{ref}	L_a/B_f	R/H_{ref}	R/B_m	D_{50}/H_{ref}
Case II	10	0.5	7	0.7	∞	∞	0.2, 0.4
					400	20	0.2, 0.4
					200	10	0.2, 0.4
			10	1.0	∞	∞	0.2, 0.4
					400	20	0.2, 0.4
					200	10	0.2, 0.4
Case III	14	0.7	4.9	0.35	∞	∞	0.2, 0.4
					400	20	0.2, 0.4
					200	10	0.2, 0.4
			7	0.5	∞	∞	0.2, 0.4
					400	20	0.2, 0.4
					200	10	0.2, 0.4
			9.8	0.7	∞	∞	0.2, 0.4
					400	20	0.2, 0.4
					200	10	0.2, 0.4
			14	1.0	∞	∞	0.2, 0.4
					400	20	0.2, 0.4
					200	10	0.2, 0.4
Case IV	20	1.0	7	0.35	∞	∞	0.2, 0.4
					400	20	0.2, 0.4
					200	10	0.2, 0.4
			10	0.5	∞	∞	0.2, 0.4
					400	20	0.2, 0.4
					200	10	0.2, 0.4
			14	0.7	∞	∞	0.2, 0.4
					400	20	0.2, 0.4
					200	10	0.2, 0.4

3.2 Design Formula for Critical Froude number for Shear Failure of Riprap Stone at Spill-
Through Abutments Placed on the Floodplains of Straight and Curved Compound Channels

For a sufficiently large channel curvature near the bridge crossing region, the flow approaching the abutments is very nonuniform as larger mean velocities develop over the outer side of the channel cross section compared to its inner side. Simulation results show that the capacity of the flow to erode the bed near the abutment and its embankments is larger for the outer-bank abutment. As the channel curvature increases, the core of high-velocity magnitude inside the main channel moves toward the outer-bank floodplain (Wu et al., 2020b).

The Year 3 report discussed the variation of the critical Froude number ($Fr = V/(gy)^{0.5}$) with D_{50}/y. Those results showed that the Pagan-Ortiz (1991) design formula is not conservative enough for the straight channel test cases considered in the present investigation. By contrast, the Lagasse et al. (2001) formula gave conservative predictions for more than half of the test cases conducted with straight channels. These test cases correspond to those for which the floodplain width is relatively small and L_a/B_f is not too high. Results also showed that for both straight and curved channel simulations, the critical Froude number decreases monotonically with increasing L_a/B_f for constant flow depth, B_f, R, and D_{50}. This effect is significant and is not taken into account by existing design equations for spill-through abutments.

Next, the focus is on proposing a design equation of the form given by eqn. (1.1) with variables C and α that adequately approximate the data set for spill-through abutments placed in both straight and curved channels. For spill through abutments, if $L_a/B_f < 1$, the characteristic length scale in the definition of the Froude number is taken as the flow depth over the floodplain, y_f. If $L_a/B_f \approx 1$, then y is equal to the flow depth in the main channel, y_m. The design equations of Pagan-Ortiz (1991) and Lagasse et al. (2001) for spill-through abutments are obtained by

21

choosing $K_s = 0.89$, $C = 0.324$, $\alpha = 2.0$ and $K_s = 0.535$, $C = 0.54$, $\alpha = 2.0$ (Fr < 0.8) in eqn. (1.1), respectively. The Year 3 report showed that a formula based on eqn. (1.1) but with variable C and α adequately fit the simulation data for spill-through abutments placed on the floodplains of a straight channel. Using a similar approach, one can propose additional C and α values that can fit the simulation data obtained in curved channels. These values are reported in table 3.2 for Cases I to IV.

Table 3.2 Best fit values of the model parameters α and C as a function of the channel radius of curvature, R, floodplain width, B_f, and relative abutment length, L_a/B_f. The last column shows predictions for Case IV using the SBR method (from Wu et al., 2020b).

	Case I $B_f/H_{ref}=5$ $B_f/B_m=0.25$	Case II $B_f/H_{ref}=10$ $B_f/B_m=0.5$	Case III $B_f/H_{ref}=14$ $B_f/B_m=0.7$	Case IV $B_f/H_{ref}=20$ $B_f/B_m=1.0$	Case IV (SBR) $B_f/H_{ref}=20$ $B_f/B_m=1.0$
$R/H_{ref}=\infty,\ R/B_m=\infty$					
$L_a/B_f=0.35$			$\alpha=1.80$ $C=0.39$	$\alpha=1.75$ $C=0.45$	$\alpha=1.75$ $C=0.75$
$L_a/B_f=0.5$		$\alpha=1.95$ $C=0.45$	$\alpha=1.80$ $C=0.45$	$\alpha=1.75$ $C=0.47$	$\alpha=1.75$ $C=0.76$
$L_a/B_f=0.7$		$\alpha=1.95$ $C=0.46$	$\alpha=1.80$ $C=0.48$	$\alpha=1.75$ $C=0.55$	$\alpha=1.75$ $C=0.77$
$L_a/B_f=1.0$	$\alpha=1.85$ $C=0.48$	$\alpha=1.85$ $C=0.59$	$\alpha=1.85$ $C=0.64$		
$R/H_{ref}=400,\ R/B_m=20$					
$L_a/B_f=0.35$			$\alpha=1.80$ $C=0.42$	$\alpha=1.75$ $C=0.48$	$\alpha=1.75$ $C=0.76$
$L_a/B_f=0.5$		$\alpha=1.95$ $C=0.45$	$\alpha=1.80$ $C=0.46$	$\alpha=1.75$ $C=0.52$	$\alpha=1.75$ $C=0.76$
$L_a/B_f=0.7$		$\alpha=1.95$ $C=0.46$	$\alpha=1.80$ $C=0.51$	$\alpha=1.75$ $C=0.61$	$\alpha=1.75$ $C=0.82$
$L_a/B_f=1.0$	$\alpha=1.85$ $C=0.55$	$\alpha=1.85$ $C=0.67$	$\alpha=1.85$ $C=0.69$		
$R/H_{ref}=200,\ R/B_m=10$					
$L_a/B_f=0.35$			$\alpha=1.80$ $C=0.44$	$\alpha=1.75$ $C=0.51$	$\alpha=1.75$ $C=0.84$
$L_a/B_f=0.5$		$\alpha=1.95$ $C=0.46$	$\alpha=1.80$ $C=0.49$	$\alpha=1.75$ $C=0.56$	$\alpha=1.75$ $C=0.95$
$L_a/B_f=0.7$		$\alpha=1.95$ $C=0.46$	$\alpha=1.80$ $C=0.54$	$\alpha=1.75$ $C=0.64$	$\alpha=1.75$ $C=1.00$
$L_a/B_f=1.0$	$\alpha=1.85$ $C=0.63$	$\alpha=1.85$ $C=0.71$	$\alpha=1.85$ $C=0.72$		

More specifically, the results in table 3.2 for Cases I to IV show that α is mainly a function of the floodplain width for test cases with $L_a/B_f < 1$. This is illustrated in figure 3.2a for the Case II simulations conducted with $B_f/H_{ref} = 10$ and $L_a/B_f \leq 0.7$. The variation of D_{50}/y with Fr is linear in log-log scale for each value of L_a/B_f. The lines corresponding to cases with $L_a/B_f = 0.5$ and 0.7 are parallel, which means that α is not a function of L_a/B_f. By contrast, the model parameter C is a function of B_f/H_{ref}, L_a/B_f, and R/H_{ref}, as shown in table 3.2. One can see that C increases monotonically with L_a/B_f for constant channel curvature if $L_a/B_f < 1$ and C increases with increasing floodplain width for constant $L_a/B_f < 1$ and channel curvature. Meanwhile, α decreases monotonically with increasing floodplain width, e.g., from 1.95 for $B_f/H_{ref} = 10$ to 1.8 for $B_f/H_{ref} = 14$ to 1.75 for $B_f/H_{ref} = 20$.
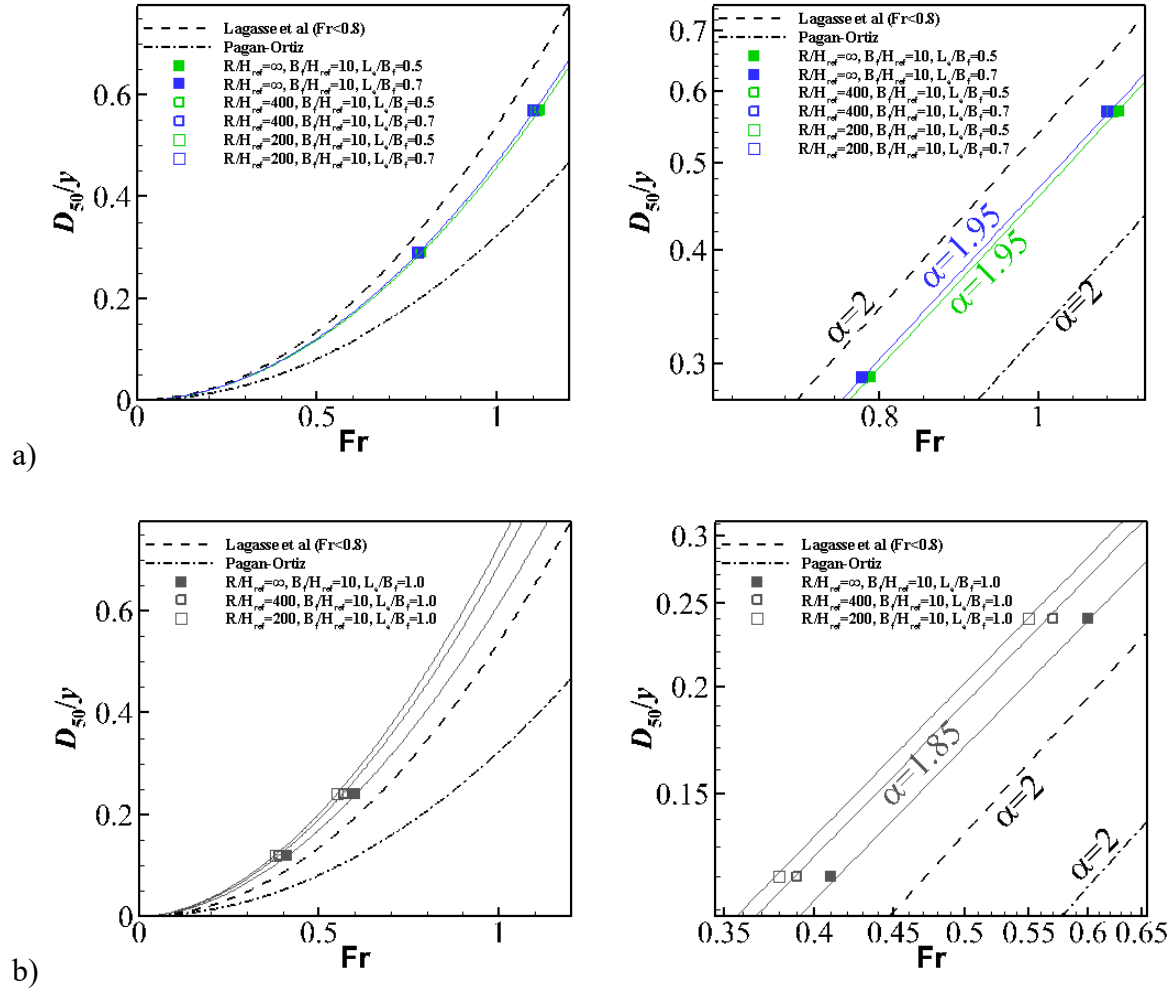
Figure 3.2 Numerical predictions of the critical Froude number for spill-through abutments with $B_f/H_{ref} = 10$ (Case II) placed in straight and curved channels. The solid lines show eqn. (1.1) predictions of the critical Froude number using the α and C values from table 3.2. a) $L_a/B_f = 0.5$ and 0.7; b) $L_a/B_f = 1$. Also shown are the Lagasse et al. (2001) and Pagán-Ortiz (1991) equations for which $\alpha = 2.0$. The right frames show the same information in log-log scale and serve to estimate the value of α for the Case II simulations with $L_a/B_f < 1$ and $L_a/B_f = 1$. From Wu et al. (2020b)

For spill-through abutments with $L_a/B_f = 1$, α is independent of the floodplain width

(table 3.2). This is illustrated in figure 3.2b that shows results for $B_f/H_{ref} = 10$ and $L_a/B_f = 1$. The

variation of D_{50}/y with Fr is linear in log-log scale and the lines are parallel with a slope $\alpha = 1.85$.

The new design formula predictions of the critical Froude number are close to the numerical results for all the cases conducted with $L_a/B_f = 0.7$ (see fig. 3.3). The qualitative trends are the same for the test cases conducted with a different value of L_a/B_f, as long as $L_a/B_f < 1$. The critical Froude number corresponding to riprap shear failure of the apron protecting the outer-bank abutment decreases with increasing channel curvature. As α is not dependent on the channel curvature, this means that C decreases with decreasing R/H_{ref} (table 3.2). Though a value of $R/B_m = 10$ ($R/H_{ref} = 200$) corresponds to a small-to-moderate channel curvature for natural streams, the effect on the critical Froude number is important. For example, in the $B_f/H_{ref} = 20$, $L_a/B_f = 0.7$, $D_{50}/H_{ref} = 0.4$ simulations, the Froude number decays from 0.97 for a straight channel to 0.85 for a curved channel with $R/H_{ref} = 200$. Also, for constant $L_a/B_f < 1$ and constant channel curvature, the Froude number decreases with increasing floodplain width.
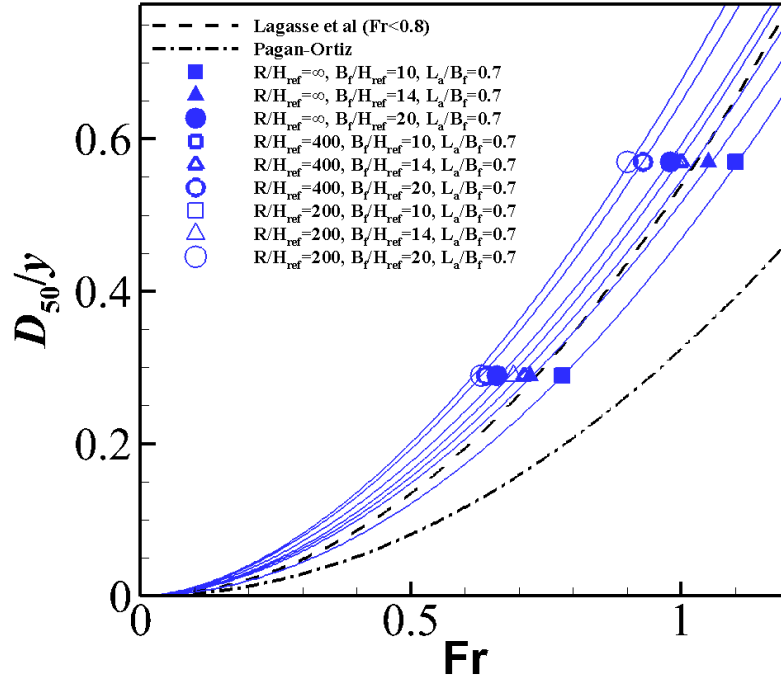
Figure 3.3 Critical Froude number as a function of floodplain width, B_f/H_{ref}, riprap size, D_{50}/y_m, and channel curvature, R/H_{ref}, for the simulations conducted with spill-through abutments with $L_a/B_f = 0.7$. The solid lines show eqn. (1.1) predictions of the critical Froude number using the α and C values from table 3.2. Also shown are the Lagasse et al. (2001) and Pagán-Ortiz (1991) equations. From Wu et al. (2020b)

The numerical predictions of the critical Froude number for the simulations conducted with $B_f/H_{ref} = 20$ and $L_a/B_f = 0.35, 0.5, 0.7$ are shown in figure 3.4. These plots contain two sets of curves and symbols. The circle symbols correspond to the critical Froude number being calculated with the mean velocity in the contracted section between the two abutments, V, and with y_f. These predictions are relatively close to those given by Lagasse et al. (2001) equation, though this equation underestimates the critical Froude number for most of the test cases with $L_a/B_f = 0.5$ and for all test cases with $L_a/B_f = 0.7$. For cases with a relatively small length of the abutment, HEC-23 (Lagasse et al. 2009) recommends using a different velocity scale that is equal to the mean velocity over the floodplain containing each abutment in the contracted section. The recommended switch from using the mean velocity in the full contracted section to

using the mean velocity over the floodplain is when the so-called set-back ratio (SBR) is larger than 5, where SBR is the ratio of the set-back length for the abutment, B_f-L_a, to the average flow depth in the channel. This switch in the definition of the velocity scale is physically sound though the threshold value SBR = 5 is somewhat arbitrary. Among the test cases considered in the present study, only Case IV test cases (fig. 3.4c) qualify for using the SBR method (SBR = 3.5 for $L_a/B_f = 0.7$ and SBR ≥ 6.0 for the lower L_a/B_f values).

a)

b)

c)
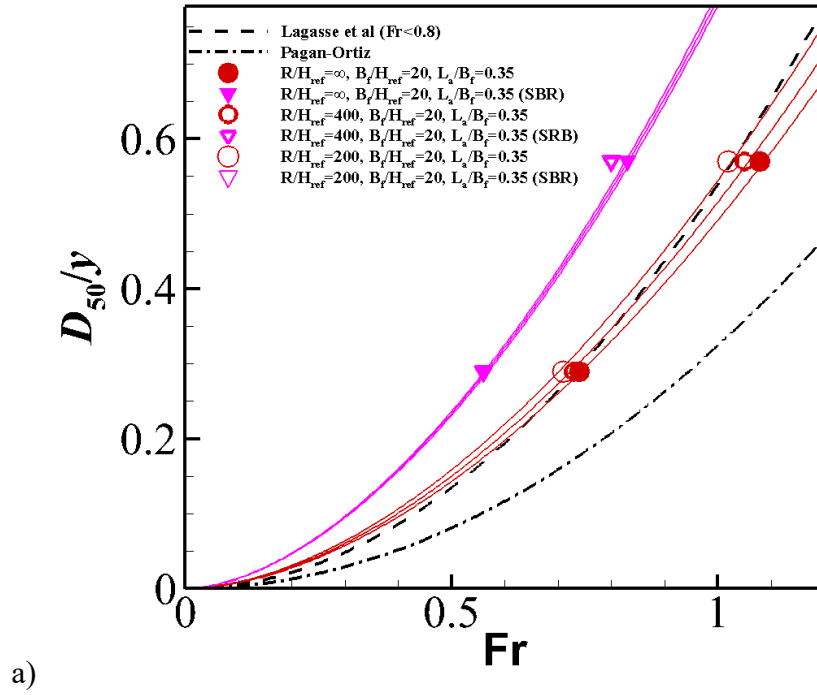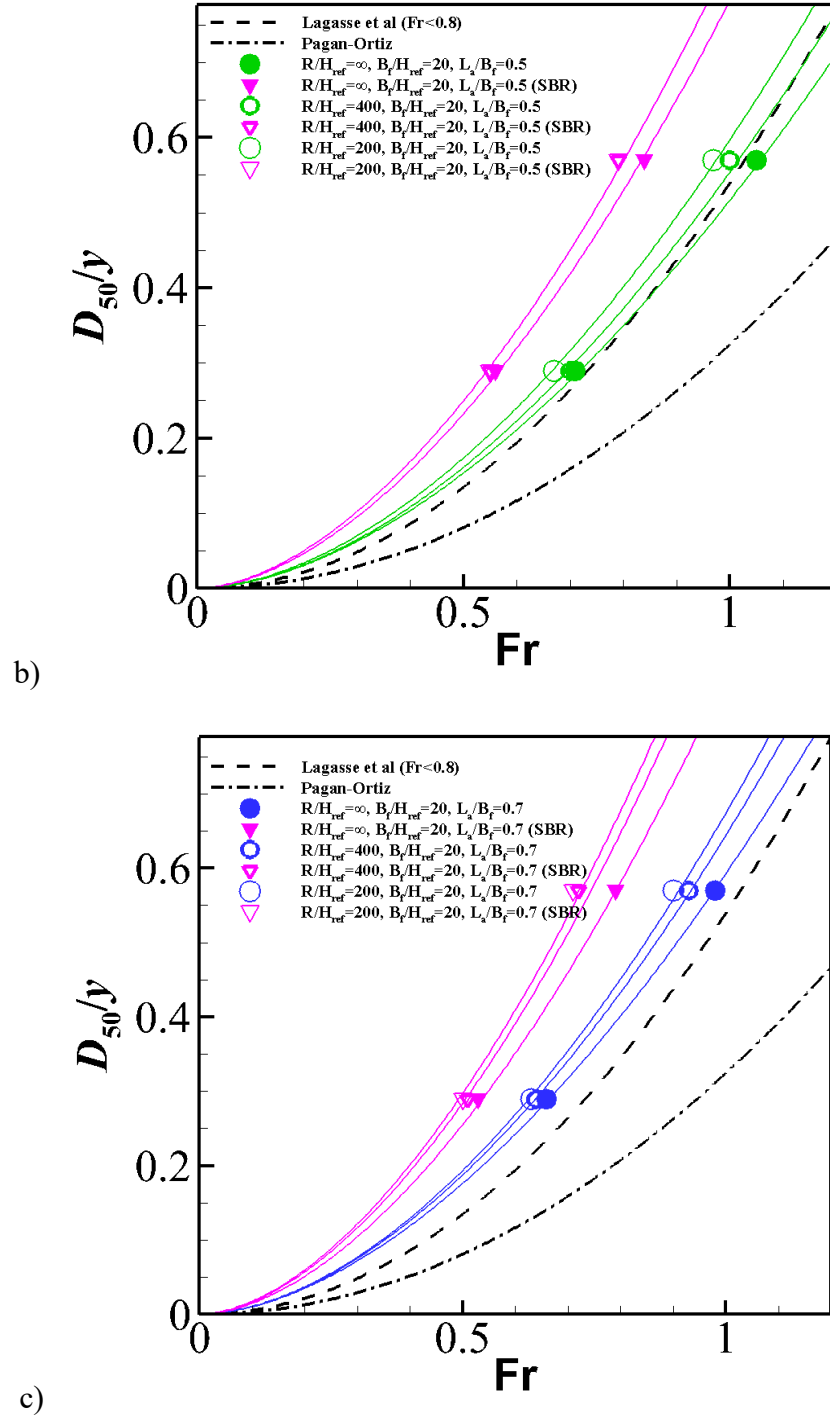
Figure 3.4 Critical Froude number as a function of relative abutment length, L_a/B_f, riprap size, D_{50}/y_m, and channel curvature, R/H_{ref}, for the Case IV simulations conducted with $B_f/H_{ref} = 20$. a) $L_a/B_f = 0.35$; b) $L_a/B_f = 0.5$; c) $L_a/B_f = 0.7$. Results are shown with the Froude number calculated using the standard method (circles) and the SBR method (triangles). The solid lines show eqn. (1.1) predictions of the critical Froude number using $\alpha = 1.75$ and the C values from table 3.2. Also shown are the Lagasse et al. (2001) and Pagán-Ortiz (1991) equations for which $\alpha = 2.0$. From Wu et al. (2020b).

The triangle symbols in figure 3.4 correspond to Froude number estimations using the SBR method. As the mean velocity over the floodplain containing the abutment is less than V, the critical Froude number calculated using the corrected velocity scale is less than the one calculated using the standard definition. One general observation is that the effect of varying the channel curvature on the critical Froude number is less strong when using the SBR method. The same procedure can be used to calculate the two parameters in the new design formula. The design equation curves adequately approximate the data when the new velocity scale is used. Interestingly, the value of the coefficient α estimated using the new velocity scale remains the same for all Case IV test cases ($\alpha = 1.75$, see table 3.2). As for calculations performed using the standard velocity scale, C increases monotonically with L_a/B_f for constant R and B_f.

Application of the new design formula requires estimation of C and α based on the geometrical variables characterizing the abutment and the channel near the bridge site. The relevant information in table 3.2 can be used to generate two new tables that allow estimating the model constants via interpolation for cases with $L_a/B_f < 1$ (table 3.3) and $L_a/B_f = 1$ (table 3.4). Table 3.3 provides the values of C and α for $0.35 \leq L_a/B_f \leq 0.9$, $10 \leq R/B_m \leq 100$, and $0.5 \leq B_f/B_m \leq 1.0$. Table 3.4 provides the values of C for $L_a/B_f = 1$, $10 \leq R/B_m \leq 100$, and $0.25 \leq B_f/B_m \leq 1.0$. For $L_a/B_f = 1$, $\alpha = 1.85$. For straight channels or for channels of very low curvature ($R/B_m > 100$), one should use the data for $R/B_m = 100$ in tables 3.3 and 3.4 to determine the values of the model parameters. For $L_a/B_f < 1$, the interpolation should first be done for L_a/B_f (only for C), then for B_f/B_m, and, finally, for R/B_m (only C).

Table 3.3 Model parameters α and C in eqn. (1.1) for spill-through abutments with $0.35 < L_a/B_f \leq 0.9$. For channels with $R/B_m < 100$, use values given for $R/B_m = 100$ (from Wu et al., 2020b).

	$B_f/B_m = 0.5$	$B_f/B_m = 0.7$	$B_f/B_m = 1.0$
	$R/B_m = 100$		
$L_a/B_f = 0.35$		$\alpha = 1.80$ $C = 0.39$	$\alpha = 1.75$ $C = 0.45$
$L_a/B_f = 0.5$	$\alpha = 1.95$ $C = 0.45$	$\alpha = 1.80$ $C = 0.45$	$\alpha = 1.75$ $C = 0.47$
$L_a/B_f = 0.7$	$\alpha = 1.95$ $C = 0.46$	$\alpha = 1.80$ $C = 0.48$	$\alpha = 1.75$ $C = 0.55$
$L_a/B_f = 0.9$	$\alpha = 1.95$ $C = 0.47$	$\alpha = 1.80$ $C = 0.51$	$\alpha = 1.75$ $C = 0.63$
	$R/B_m = 20$		
$L_a/B_f = 0.35$		$\alpha = 1.80$ $C = 0.42$	$\alpha = 1.75$ $C = 0.48$
$L_a/B_f = 0.5$	$\alpha = 1.95$ $C = 0.45$	$\alpha = 1.80$ $C = 0.46$	$\alpha = 1.75$ $C = 0.52$
$L_a/B_f = 0.7$	$\alpha = 1.95$ $C = 0.46$	$\alpha = 1.80$ $C = 0.51$	$\alpha = 1.75$ $C = 0.61$
$L_a/B_f = 0.9$	$\alpha = 1.95$ $C = 0.47$	$\alpha = 1.80$ $C = 0.56$	$\alpha = 1.75$ $C = 0.70$
	$R/B_m = 10$		
$L_a/B_f = 0.35$		$\alpha = 1.80$ $C = 0.44$	$\alpha = 1.75$ $C = 0.51$
$L_a/B_f = 0.5$	$\alpha = 1.95$ $C = 0.46$	$\alpha = 1.80$ $C = 0.49$	$\alpha = 1.75$ $C = 0.56$
$L_a/B_f = 0.7$	$\alpha = 1.95$ $C = 0.46$	$\alpha = 1.80$ $C = 0.54$	$\alpha = 1.75$ $C = 0.64$
$L_a/B_f = 0.9$	$\alpha = 1.95$ $C = 0.46$	$\alpha = 1.80$ $C = 0.59$	$\alpha = 1.75$ $C = 0.72$

Table 3.4 Model parameter C in eqn. (1.1) for spill-through abutments with $L_a/B_f = 1$ for which $\alpha = 1.85$. For channels with $R/B_m < 100$, use values given for $R/B_m = 100$ (from Wu et al., 2020b)

	$B_f/B_m = 0.25$	$B_f/B_m = 0.5$	$B_f/B_m = 0.7$	$B_f/B_m = 1.0$
$R/B_m = 100$	$C = 0.48$	$C = 0.59$	$C = 0.64$	$C = 0.69$
$R/B_m = 20$	$C = 0.55$	$C = 0.67$	$C = 0.69$	$C = 0.71$
$R/B_m = 10$	$C = 0.63$	$C = 0.71$	$C = 0.72$	$C = 0.73$

Chapter 4 Effect of pressurized-flow conditions on bed shear stress distributions and critical Froude number for riprap aprons protecting wing-wall abutments placed in a straight compound channel

The other major research activity conducted during Year 4 was to perform VOF simulations of flow in a straight channel containing wing-wall abutments (fig 4.1). New meshes were generated for simulations with VOF in which a layer of air was included at the top of the computational domain. Simulations were conducted with different flow depths in the approach flow and diameters of the riprap stone for cases when the bridge deck supported by the abutments is fully (overtopping flow regime, OT) or partially submerged (submerged orifice flow regime, SO). The goal of these simulations is to investigate how the critical discharge and the critical Froude number corresponding to entrainment of riprap stone of a certain size decrease with increasing water elevation upstream of the abutments. Simulations were also conducted with the same incoming flow depths but without a bridge deck to be able to quantify the effect of pressurized flow conditions beneath the bridge deck on the critical discharge and critical Froude number corresponding to shear failure of the riprap stone.

Due to the symmetry of the problem, the computational domain contained only half of the channel and one abutment (fig. 4.1). Simulations were conducted with a bridge deck of thickness d_{bd}=0.01 m and width 0.5 m. The thickness of the region containing the bridge beams was d_{bb}=0.02 m and its width was 0.4 m. The distance between the channel bottom and the bottom of the region containing the bridge beams was 0.18 m. As for the simulations conducted with a flow depth of 0.17 m (free surface flow regime at the bridge site), the width of the main channel was W=2 m. The channel half width was 1 m. The floodplain width was B_f=0.4 m.
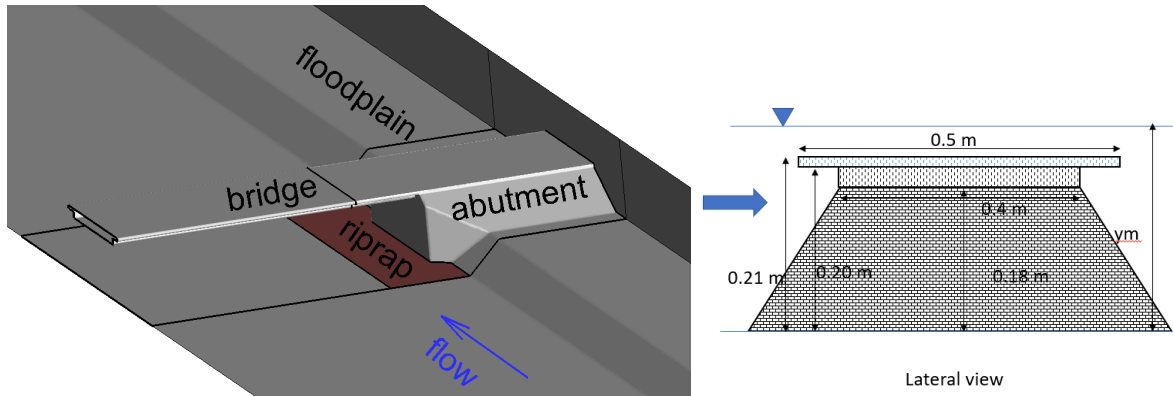
Figure 4.1 Sketch showing computational domain containign the wing-wall abutment and cross section cutting through the abutment and the bridge deck.
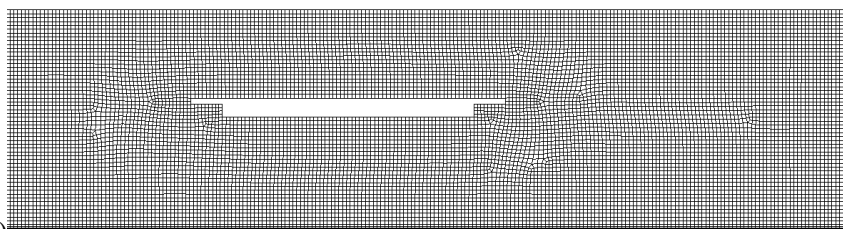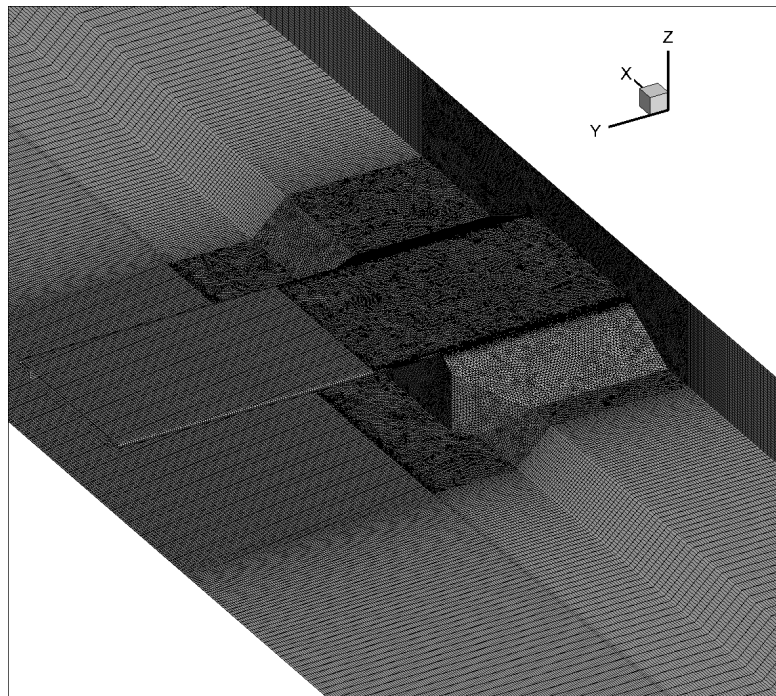
Figure 4.2 Computational mesh used in the VOF simulations of flow past wing-wall abutments placed in a straight channel (y_m=0.22 m). a) 3-D view showing mesh on the different surfaces; b) vertical cut through the bridge deck.

The abutment (fig. 4.1) was identical to the one used in rigid-lid simulations that were used in Year 2 to obtain a new two-parameter design formula for riprap sizing at wing-wall abutments. The abutment has a trapezoidal cross section and its extremity slightly penetrates into the main channel. The slope of the sidewalls are 1V:2H and the bottom width of the abutment is 0.9 m. As discussed by Melville et al. (2007), this abutment is representative of a four-lane highway bridge at a scale close to 1:20. Figure 4.2 shows the computational mesh used in the VOF simulations. A layer of air is present above the water domain, so the height of the computational domain is significantly larger than y_m.
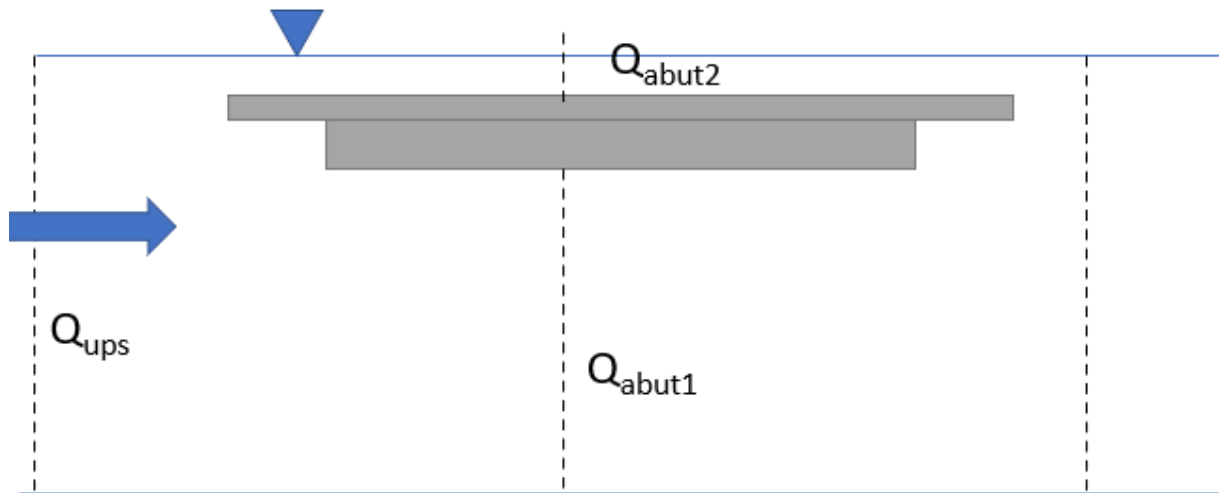
Figure 4.3 Sketch showing main flow variables for the case when the flow depth upstream of the abutment is sufficiently large for the bridge deck to become submerged.

Simulations in channels containing wing-wall abutments at their sides were performed with the same value of the mean sand diameter (d_{50}=0.00082 m) but with different values of the mean riprap stone diameter, D_{50}=0.061 m, 0.04 m, and 0.028 m. The total streamwise length of the riprap apron was 1.35 m, with riprap stone being present starting 0.5 m upstream of the abutment and ending 0.35 m downstream of it. The width of the riprap apron protecting the

outer-bank abutment was 0.5 m. For each case, simulations were performed with different values of the inlet discharge until the maximum value of the bed friction velocity over the riprap region was equal to $u_{\tau c}$. This value is denoted as Q_{ups}. If the free surface reaches the bridge deck, then Q_{ups} has two components (Q_{abut1} and Q_{abut2}), as shown in figure 4.3. The part of the total discharge, Q_{upsc}, advected beneath the bridge deck at critical conditions is denoted Q_{abut1c}. A critical Froude number, Fr', can be defined with Q_{ups} and y_{ups}, where y_{ups} is the constant flow depth upstream of the bridge deck.

The VOF module was validated and then applied to estimate the critical channel discharge and the corresponding critical Froude number for different values of riprap size (0.028 m<D_{50}<0.06 m) and incoming flow depth in the main channel 0.17 m<y_m<0.24 m. The matrix of simulations is given in table 4.1. The numerically predicted critical total discharge and the discharge beneath the bridge deck are given in table 4.2. The same table shows the critical Froude number, Fr', for each case.

Table 4.1 Matrix of test case for flow in a straight channel with a bridge containing two wing-wall abutments.

Case	Pressure flow types	Main-channel initial depth y_m (m)	Floodplain initial depth y_f (m)	Riprap stone size D_{50} (m)
Group 1 With bridge deck ($\tau_{max} = \tau_c$)	Free surface (FS)	0.17	0.07	0.028
				0.04
				0.061
	Submerged orifice (SO)	0.195	0.095	0.028
				0.04
				0.061
	SO~OT	0.205	0.105	0.028
				0.04
				0.061
	Overtopping (OT)	0.22	0.12	0.028
				0.04
				0.061
	Overtopping (OT)	0.24	0.14	0.028
				0.04
				0.061

Case	Main-channel initial depth y_m (m)	Floodplain initial depth y_f (m)	Riprap stone size D_{50} (m)
Group 2 No bridge deck ($\tau_{max} = \tau_c$)	0.195	0.095	0.028
			0.04
			0.061
	0.205	0.105	0.028
			0.04
			0.061
	0.22	0.12	0.028
			0.04
			0.061
	0.24	0.14	0.028
			0.04
			0.061
Group 3 No bridge deck (use Q_c from group 1)	0.195	0.095	0.028
			0.04
			0.061
	0.205	0.105	0.028
			0.04
			0.061
	0.22	0.12	0.028
			0.04
			0.061
	0.24	0.14	0.028
			0.04
			0.061

Table 4.2 Main parameters predicted at critical conditions for the simulations with $y_m=0.17$ m, $y_m=0.22$ m and $y_m=0.24$ m. See also Fig. 4.3.

y_m (m)	D_{50} (mm)	y_{ups} (m)	D_{50}/y_{ups} (-)	$u_{\tau c}$ (m/s)	$u_{\tau max}/u_{\tau c}$ (-)	Q_{upsc} (m³/s)	Q_{abut1c} (m³/s)	Q_{abut1c}/Q_{upsc} (-)	Fr'
0.17	28	0.17	0.165	0.058	1	0.088	0.088	1.00	0.432
0.17	40	0.18	0.222	0.07	1	0.100	0.101	1.01	0.491
0.17	61	0.18	0.339	0.084	1	0.122	0.122	1.00	0.598
0.195	28	0.191	0.147	0.058	1	0.094	0.081	0.86	0.391
0.195	40	0.203	0.197	0.07	1	0.113	0.099	0.88	0.455
0.195	61	0.208	0.293	0.084	1	0.132	0.118	0.90	0.549
0.205	28	0.203	0.138	0.058	1	0.096	0.080	0.83	0.383
0.205	40	0.21	0.190	0.07	1	0.115	0.100	0.87	0.429
0.205	61	0.216	0.282	0.084	1	0.142	0.124	0.87	0.531
0.22	28	0.221	0.127	0.058	1	0.096	0.073	0.76	0.311
0.22	40	0.228	0.175	0.07	1	0.122	0.099	0.81	0.413
0.22	61	0.234	0.261	0.084	1	0.150	0.129	0.86	0.516
0.24	28	0.24	0.117	0.058	1	0.105	0.077	0.73	0.305
0.24	40	0.252	0.159	0.07	1	0.148	0.109	0.74	0.422
0.24	61	0.258	0.236	0.084	1	0.173	0.132	0.76	0.510

Simulation results show that the core of high streamwiswe velocity moves closer to the bed as the flow becomes pressurized (fig. 4.4) and the size of the region of relatively high bed shear stress over the riprap apron increases (e.g., it penetrates until the lateral edge of the riprap apron) as the flow accelerates beneath the bridge deck (fig. 4.5). Free surface effects are particularly strong in the $y_m=0.24$ m simulation shown in figure 4.4b. As expected, some of the incoming flow moves over the top of the bridge deck. A standing wave is generated near the upstream edge of the bridge deck and the free surface waviness is significant for a streamwise distance of about 3-4 times the width of the bridge deck. Over the bridge deck and downstream of it, the streamwise velocity is relatively high near the free surface. This effect increases monotonically with decreasing D_{50}.
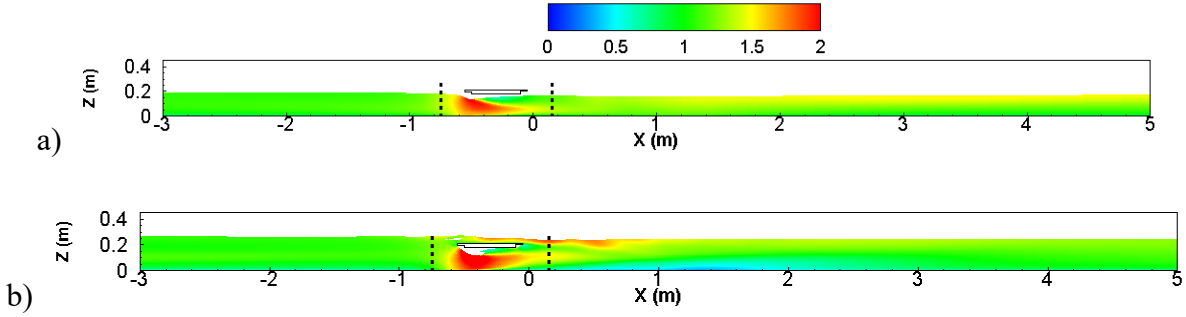
Figure 4.4 Normalized streamwise velocity distribution in a streamwise-vertical cross section situated close to the front edge of the wing-wall abutment. Riprap size is D_{50}=0.061 m and B_f=0.4 m. a) open channel flow y_m=0.17 m; b) pressurized flow, y_m=0.24 m.
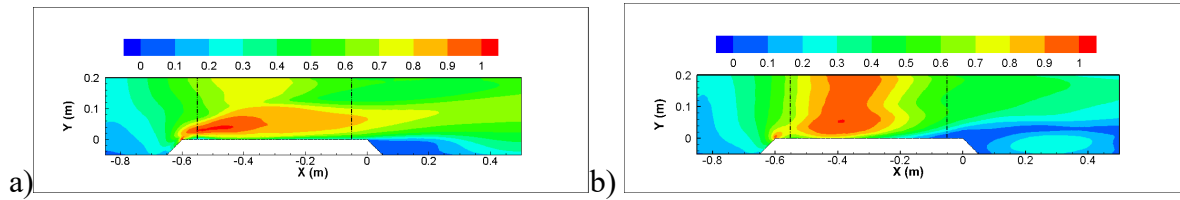
Figure 4.5 Normalized bed shear stress, τ/τ_{max}, over the riprap region at critical entrainment conditions where $\tau_{max}=\tau_{cr}$ (D_{50}=0.061 m, B_f=0.4 m). a) free surface flow regime, y_m=0.17 m; b) overtopping flow regime, y_m=0.24 m.

With respect to the corresponding free surface flow regime case (y_m=0.17 m, fig. 4.5a), another region of relatively high velocity magnitude forms in between the bottom of the bridge deck and the channel bottom. The presence of such a region has direct consequences on the capacity of the flow to entrain sediment beneath the bridge deck due to pressure scour effects, including inside the subregion where the riprap apron is present. The level of velocity amplification inside this region increases monotonically with increasing D_{50}.

The velocity magnitude distributions in a horizontal plane situated midway between the bottom of the bridge deck and the channel bottom shown in figure 4.6 allow to better understand the effects of the flow becoming pressurized beneath the bridge deck on the capacity of the flow to entrain sediment in the same region. The region of velocity amplification extends over the

whole region situated in between the lateral extremities of the two abutments. This region is

larger, and the area of relatively high velocities extends until the symmetry plane of the main

channel in the simulation conducted with D_{50}=0.061 m. As D_{50} decreases, the size of the region

of high streamwise velocities near the symmetry plane decreases. For all values of D_{50}, the larger

velocities are situated closer to the lateral edge of the abutment, with the peak values occurring

close to the upstream corner of the vertical face of the abutment. This is due to the high

amplification of the streamwise velocity as it passes the upstream corner of the abutment. The

velocity field recovers slower toward values that are close to the inlet velocity in the simulation

conducted with D_{50}=0.061 m compared to the simulation conducted with D_{50}=0.028 m. This

means that the capacity of the flow to entrain sediment inside the main channel beneath and

downstream of the bridge deck increases with D_{50}. The opposite is true over the floodplains.
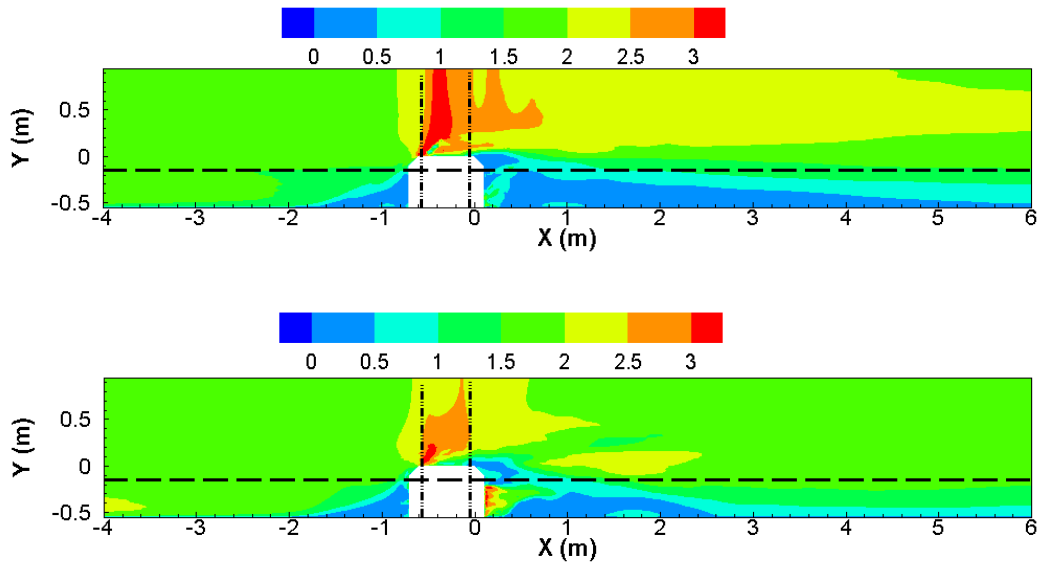
Figure 4.6 Nondimensional velocity magnitude, U_{mag}/U_{inlet}, in horizontal plane cutting midway between the channel bottom and the bottom of the bridge deck (z=0.12 m) for critical entrainment conditions, where U_{inlet} is the mean velocity at the inlet section. a) y_m=0.22 m, D_{50}=0.061 m; b) y_m=0.22 m, D_{50}=0.028 m. The dash-dotted lines show the position of the bridge deck. The dash line shows the start of the transition region between the floodplain and the main channel.
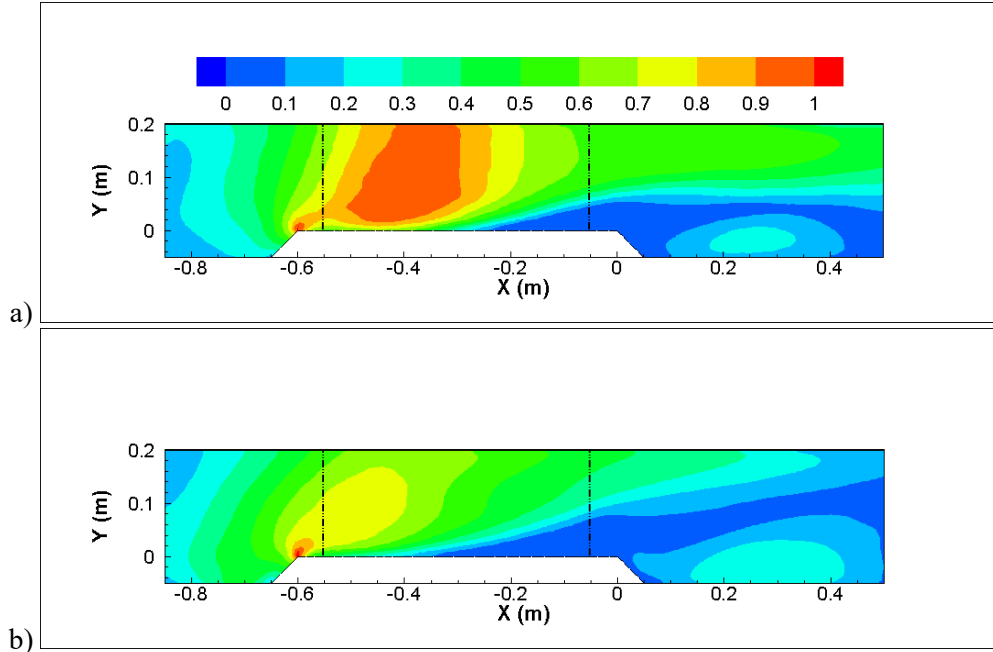
Figure 4.7 Nondimensional bed shear stress distributions predicted over the riprap region, τ/τ_{max}, at critical entrainment conditions where $\tau_{max}=\tau_{cr}$ for a given value of the riprap stone diameter D_{50}. a) y_m=0.22 m, D_{50}=0.061 m; b) y_m=0.22 m, D_{50}=0.028 m. The dash-dotted lines show the position of the bridge deck.

Figure 4.7 compares the nondimensional bed shear stress distributions over the riprap region at critical flow conditions in the y_m=0.22 m simulations conducted with different values of D_{50}. As for the case when the free surface is situated beneath the bridge deck, the peak value of the bed shear stress occurs at the upstream corner of the lateral face of the abutment. At this location, τ/τ_{max}=1. Consistent with the velocity distributions in figure 4.6, bed shear stresses that are comparable to the peak values are predicted over a relatively large part of the riprap apron situated beneath the bridge deck in the simulation conducted with D_{50}=0.061 m. So, once the flow conditions are such that the bed shear stress becomes larger than the critical value for riprap failure, one should expect that most of the riprap stone situated beneath the bridge deck is going to be entrained by the overflow due to pressure scour effects. By contrast, in the simulation conducted with D_{50}=0.028 m, the values of the nondimensional bed shear stress decay rapidly

away from the upstream corner of the abutment. This effect is mostly a consequence of the fact that increasing D_{50} results in an increase of the percentage of the incoming flow advected beneath the bridge deck.

To better understand the effect of the flow becoming pressurized in the simulations where the water surface is situated above the bottom of the bridge deck, additional simulations were conducted with the same value of y_m but without a bridge deck. The matrix of these simulations is also given in table 4.2. For y_m=0.24 m, the ratio between the peak bed shear stress over the riprap apron and the critical value for riprap entrainment was equal to 0.85 for D_{50}=0.04 m and to 0.8 for D_{50}=0.061 m. This shows that once the flow becomes pressurized, its capacity to induce sediment entrainment increases significantly. Simulations without a bridge deck were also conducted with the same values of y_m to determine the critical discharge (table 4.2). For example, for y_m=0.24 m, the ratio between the critical discharges in the corresponding simulations with no bridge deck and with bridge deck was 1.22 for D_{50}=0.04 m and 1.31 for D_{50}=0.061 m.

Some of the simulations parts of groups 2 and 3 in table 4.2 are still being completed. Once all the data are available and postprocessed, the goal will be to understand the effect of the occurrence of pressurized flow conditions (OT or SO regimes) on the relationship between the critical number, Fr', and the nondimensinal riprap diameter, D_{50}/y_{ups}. This analysis will be completed during Year 5.

Chapter 5 Conclusions and Proposed Future Work

As part of the present research project, a general methodology based on fully 3-D, non-hydrostatic RANS numerical simulations was developed to determine the conditions for riprap shear failure for cases when a riprap apron is placed close to an abutment in a compound channel. The relationship proposed by Melville and Coleman (2000) and Melville et al. (2007) for riprap entrainment threshold (shear failure mode) was used to determine if riprap stone entrainment occurs. The methodology was validated during Year 1 for wing-wall abutments using the experimental data of Melville et al. (2007). Based on data obtained using this methodology, a new riprap sizing design formula was proposed for wing-wall abutments in Year 2. The proposed numerical approach is much less expensive compared to the classical one based on laboratory scaled-model investigations and allows incorporating additional complexities present at many bridge sites.

A main finding of the study carried during Year 3 for spill-through abutments placed in a compound straight channel was the data generated via numerical simulations showed the Lagasse et al. (2001) formula gave more accurate predictions compared to the Pagan-Ortiz (1991) formula. Still, even the Lagasse et al. (2001) formula overpredicted the critical value of the Froude number for test cases conducted with high values of the floodplain width (e.g., B_f=2.0 m). Slight overpredictions were observed, even for smaller values of B_f, if the relative length of the abutment, L_a/B_f, was sufficiently large. The critical Froude number was found to decay monotonically with the decrease in L_a/B_f, an effect not accounted for in any existing design formulas.

The main outcome of the research performed during Year 4 was a new, two-parameter riprap sizing formula for protection of spill-through abutments against erosion. The formula can

be used in both straight and curved compound channels with a radius of curvature of the main channel, R, that is less than 10 times the channel width, B_m. This significantly enlarges the range of practical conditions where the new formula can be applied, as many bridges are built in regions where the channel curvature is not negligible. The formula retains the functional relationship ($D_{50}/y = C^{0.5\alpha} * Fr^\alpha$) of the Lagasse et al. (2001) and Pagan-Ortiz (1999) formulas used for riprap apron design at wing-wall and spill-through abutments. The present numerical predictions were able to understand the effects of the various geometrical parameters (e.g., floodplain width, channel radius of curvature, relative abutment length) on the critical Froude number needed to avoid shear failure of riprap stone of a given diameter. Standard design formulas do not incorporate the effects of all these variables on the critical value of the Froude number that will result in riprap entrainment. Increasing channel curvature was found to further reduce the critical Froude number at which riprap shear failure occurs at the outer-bank, spill-through abutment. So, to provide accurate predictions for such cases, the model parameters should also be a function of R.

Analysis of the simulation data showed that α is only a function of the floodplain width for cases where L_a is not very close to B_f and the apron does not extend into the main channel. The predicted values of α ($1.75 \leq \alpha \leq 1.95$) for the test cases with $L_a/B_f < 1$ were slightly lower than that ($\alpha = 2$) used in the design formulas of Lagasse et al. (2001) and Pagan-Ortiz (1991). Moreover, α was found to decay monotonically with increasing floodplain width. Finally, for cases with $L_a/B_f = 1$, where the riprap shear failure occurs over the part of the apron situated inside the main channel, one should use $\alpha = 1.85$ independent of the floodplain width. The new design formula was found to adequately fit all the data sets generated via numerical simulations.

The other main outcome of Year 4 was to develop and test a new version of the 3-D

RANS numerical model that can be used to predict bed shear stress distributions over the apron

region for cases when the free surface elevation needs to be computed as part of the solution.

This is a requirement to study cases when the free surface interacts with the bridge deck.

Simulations with a deformable free surface using the Volume of Fluid method were performed

given that the rigid lid approximation is no longer valid for pressurized flow simulations. The

focus was on a wing wall abutment protected by a riprap apron (0.028 m$<D_{50}<0.061$ m) that is

situated in a straight compound channel. Besides the wing wall abutment, the bridge deck was

part of the computational domain.

Simulations covered a wide range of relevant cases. With increased flow depth in the

incoming flow, the flow regime near the bridge deck connecting the two abutments changed

from free surface (FS) flow to submerged orifice (SO) flow and then to (bridge-deck)

overtopping (OT) flow. Simulations conducted with SO and OT flow at the bridge site were

found to be characterized by very complex patterns of the velocity and bed shear stress

distributions inside the pressurized-flow region and downstream of it. Simulation results showed

that the core of high streamwiswe velocity moved closer to the bed as the flow became

pressurized. Meanwhile, the size of the region of relatively high bed shear stress over the riprap

apron increased (e.g., it penetrated up to the lateral edge of the riprap apron) as the flow

accelerated beneath the bridge deck. The numerical model was then used to predict how the

critical Froude number and critical discharge defined using the flow depth in the approaching

flow, y_{ups}, varied as the elevation of the free surface increased.

During Year 5, further analysis of the data sets generated for wing-wall abutments placed

in a straight channel will be undertaken to understand how the critical Froude number is affected

by pressurized flow effects. The goal will be to propose corrections to existing design formulas that can be used only for free surface flow regime. The second main objective of Year 5 will be to follow a similar approach to investigate how the critical Froude number varies for riprap aprons protecting spill-through abutments placed on the floodplains of a straight compound channel and to propose corrections that can be used to determine the critical Froude number for cases when the submerged orifice flow regime or the overtopping flow regime are observed at the bridge site. For pressurized flow cases, corresponding simulations will be conducted with no bridge deck to estimate the effects of the pressurized flow regime on the critical Froude number, maximum bed shear stress and critical discharge.

We will work with the Transportation Research Board committee TRB-AFB60 such that the main findings and the proposed new design formulas for determining minimum riprap size at wing-wall and spill-through abutments will be considered for adoption in a future FHWA Technical Brief update to HEC 23. Once adopted, the new procedure will enhance the capabilities of state DOTs to develop more reliable approaches to protect bridges against possible failure induced by severe erosion associated with flood events. At a more general level, more accurate riprap design formulas for protection of abutments against erosion will result in significant reduction of the costs to operate roads during and after flood events. It will also contribute to reducing the risk for hazards associated with bridge failure during floods by avoiding structural failure.

References

Barkdoll, B. D., Ettema, R., & Melville, B. W. (2007). *Countermeasures to protect bridge abutments from scour* (NCHRP Project 24-18. NCHRP Report 587). Transportation Research Board.

Brown, S. A., & Clyde, E. S. (1989). *Design of riprap revetment: Hydraulic Engineering Circular No. 11* (FHWA-IP-016). National Highway Institute (US).

Cardoso, A., Simarro, G. and Schleiss, A. (2010). *Sizing of riprap for spill-through abutments, Water Management*, 163, issue WM10, 499-507, Paper 900024.

Cheng, Z., Koken, M. and Constantinescu, G. (2018). Approximate methodology to account for effects of coherent structures on sediment entrainment in RANS simulations with a movable bed and applications to pier scour. *Advances in Water Resources,* 120, 65-82.

Chiew, Y. M. (1995). Mechanics of riprap failure at bridge piers. *Journal of Hydraulic Engineering*, *121*(9), 635-643.

Dey, S. & Barbhuiya, A.K. (2005). Time variation of scour at abutments. *Journal of Hydraulic Engineering, 131(1),* 11-23.

Ettema, R, Constantinescu, G and Melville, B. (2011). *NCHRP 24-27(01): Evaluation of bridge pier scour research: scour processes and estimation*. Final report for NCHRP.

Ettema, R., Ng, K., Chakradhar, R., Fuller, J., & Kempema, E. W. (2015). Failure of spill-through bridge abutments during scour: Flume and field observations. *Journal of Hydraulic Engineering, 141(5),* 06015001.

Ettema, R., Constantinescu, G., & Melville, B. W. (2017). Flow-field complexity and design estimation of pier-scour depth: Sixty years since Laursen and Toch. *Journal of Hydraulics Engineering*, *143*(9), 03117006.

Hoffmans, G. J., & Verheij, H. J. (1997). *Scour manual* (Vol. 96). A.A. Balkema, Rotterdam, Netherlands.

Hong, S. H., and Abid, I. (2019). Scour around an erodible abutment with riprap apron over time. *Journal of Hydraulic Engineering, 145(6),* 06019007.

Horna-Munoz, D. and Constantinescu, G. (2018). A fully 3-D numerical model to predict flood wave propagation and assess efficiency of flood protection measures. *Advances in Water Resources, 122*, 148-165.

Horna-Munoz, D. and Constantinescu, G. (2020) 3-D dam break flow simulations in simplified and complex domains, *Advances in Water Resources*, *137*, 103510, https://doi.org/10.1016/j.advwatres.2020.103510.

Koken, M., & Constantinescu, G. (2014). Flow and turbulence structure around abutments with sloped sidewalls. *Journal of Hydraulic Engineering*, *140*(7). 04014031.

Kothyari, U.C., Hager, W.H. and Oliveto, G. (2007). Generalized approach for clearwater scour at bridge foundation elements, *Journal Hydraulic Engineering, 133(11),* 1229-1240.

Lagasse, P, Zevenberger,L., Schall, J and Chopper, P. (2001). *Bridge scour and stream instability countermeasures: experience, selection, and design guidance: Hydraulic Engineering Circular No. 23* (FHWA-NH1-01-003). National Highway Institute (US).

Lagasse, P. F., Clopper, P. E., Pagán-Ortiz, J. E., Zevenbergen, L. W., Arneson, L. A., Schall, J. D., & Girard, L. G. (2009). *Bridge scour and stream instability countermeasures: experience, selection, and design guidance: Hydraulic Engineering Circular No. 23* (FHWA-NHI-09-111). National Highway Institute (US).

Melville, B. W. and Coleman, S. E. (2000). *Bridge scour.* Water Resources Publications, Littleton, Colorado.

Melville, B., van Ballegooy, S., Coleman, S. and Barkdoll, B. (2006a). Countermeasures to protection at spill-through abutments. *Journal of Hydraulic Engineering, 132*:235-245.

Melville, B., van Ballegooy, S., Coleman, S. and Barkdoll, B. (2006b). Scour countermeasures for wing wall abutments. *Journal of Hydraulic Engineering, 132*:563-574.

Melville, B., Van Ballegooy, S., Coleman, S. and Barkdoll, B. (2007). Riprap selection at wing wall abutments. *Journal of Hydraulic Engineering,133*:1265-1269.

NCHRP Project 24-18 (*NCHRP Report 587*), *Countermeasures to Protect Bridge Abutments from Scour.*

NCHRP Project 24-19, *Selection Criteria and Design Guidelines, and techniques for the Size and Placement of Environmentally Sensitive Channel and Bank Protection Measures, and Quality Control.*

NCHRP Project 24-20, *Prediction of Scour at Bridge Abutments*.

Pagaz-Ortiz, J. (1991). *Stability of rock riprap for protection at the toe of abutments located at the flood plain, Rep. No. FHWA-Rd-91-057*, Federal Highway Administration, US Dept. of Transportation, Washington, DC.

Roulund, A., Sumer, M., Fredsoe, J. ad Michelsen, J. (2005). Numerical and experimental investigations of flow and scour around a circular pile. *Journal of Fluid Mechanics, 534,* 351-401.

Sturm, T. W., & Janjua, N. S. (1994). Clear water scour around abutments in floodplains. *Journal of Hydraulic Engineering, 120*(8), 956-972.

Sturm, T. W., Ettema, R., & Melville, B. W. (2011). *Evaluation of bridge-scour research: Abutment and contraction scour processes and prediction (pp. 24-27).* Washington, DC, USA: National Cooperative Highway Research Program, Transportation Research Board of the National Academies.

Sumer, B. M. and Fredsoe J. (2002). *The mechanics of scour in the marine environment*. World Scientific.

Wu, H., Zeng, J. and Constantinescu, G. (2020a). A multi-parameter design formula for riprap size selection at wing-wall abutments, *Journal Hydraulic Research*, paper TJHR-2019-0218, https://doi.org/10.1080/00221686.2020.1818310.

Wu, H., Zeng, J. and Constantinescu, G. (2020b). A design formula for sizing rock riprap at spill-through abutments in compund channels, *Journal Hydraulic Engineering*, 147(10), https://doi.org/10.1061/(ASCE)HY.1943-7900.0001919.

Zeng, J., Constantinescu, G., Blanckaert, K., & Weber, L. (2008). Flow and bathymetry in sharp open-channel bends: Experiments and predictions. *Water Resources Research*, *44*(9), W09401.